

Feasibility of dry cooling in supercritical CO₂ power cycle in concentrated solar power application: Review and a case study

M. Monjurul Ehsan ^{*}, Zhiqiang Guan, Hal Gurgenci, Alexander Klimenko

Renewable Energy Conversion Centre of Excellence, School of Mechanical and Mining Engineering, The University of Queensland, Brisbane, QLD, 4072, Australia



ARTICLE INFO

Keywords:
 Supercritical CO₂
 Dry cooling
 Concentrated solar power
 Cooling tower
 Recompression
 Partial cooling

ABSTRACT

Past research intensely stressed the application of supercritical CO₂ (sCO₂) in power cycles for large-scale electricity generation in the near future by adapting decarbonization policy with clean energy technologies. The prominent closed-loop sCO₂ Brayton cycle has all the potential for the future power generation over the traditional superheated/supercritical Rankine cycle for concentrated solar power applications. Using sCO₂ as a working fluid has been preferred as one of the most efficient and environmentally safe alternatives over the traditional refrigerants and other working fluids. While the thermodynamic analysis of sCO₂ cycles has been in a great number of recent studies, its particular advantages when coupled with dry cooling have not been adequately analyzed. The sCO₂ power cycle efficiency is highly influenced by the cycle lowest temperature, hence cooling system design significantly impacts the cycle performance. In the present work, the applicability and the potential benefits of the dry cooling system are demonstrated for sCO₂ cycles over the traditional Rankine cycle. The detailed thermodynamic modelling of the dry cooling system is presented. Research studies on dry cooled sCO₂ power cycles are reviewed with their major findings. Various techniques are identified from the literature to compensate for the efficiency degradation of the power cycle during high ambient temperature. The implementation of the extremum seeking controller, the hybrid cooling, and the radiative cooling option certainly can improve the cycle performance at the off-design condition. A thermodynamic analysis is performed to design the cooling tower for recompression and the partial cooling cycles. The nodal approach adapted in the present work allows predicting the radical variation of transport properties inside the tubes of the heat exchanger. The towers are designed based on the optimum operating condition of the power cycle. The cycle performance is investigated with the variation sCO₂ entrance temperature into the cooling system and the ambient temperature. This case study shows a pathway in designing the cooling system for sCO₂ power cycles. This review work highly emphasizes the potential benefits of dry cooling in sCO₂ power cycles and presents the cooling system design methodology for efficient cycle operation.

1. Introduction

1.1. The global energy crisis

The rapid industrial revolution, technological advancement, and population growth have led to a serious concern in resolving the global energy crisis and lessening the greenhouse concentration level by adapting decarbonization policies for power generation and industrialization. The international energy agencies and policymakers are working towards the development of renewable and sustainable energy technologies to alleviate the perishable fossil fuel resources and improve the overall energy conservation. Renewable energies are inexhaustible,

clean, and environmentally friendly, and technological development with renewable energy is a prominent area of research. Recent research studies suggest substantial scientific progress in concentrated solar power (CSP) serves as a potential renewable energy technology for the next generation clean power generation. The various power conversion thermodynamic cycles can be integrated with CSP equipped with thermal energy storage that provides dispatchable power generation.

1.2. Energy statistics in Australia

Concerns on climate change motivate a concerted effort towards reducing greenhouse gas emissions through decarbonization of power

* Corresponding author.

E-mail address: m.ehsan@uqconnect.edu.au (M.M. Ehsan).

generation. Renewable power is an option but the intermittency of the renewable source emphasizes the need for energy storage as the renewable power penetration into the power networks increases. Concentrated solar power holds a particular promise in this context because solar heat is easier to store than electricity and stored heat can be converted to electricity when there is demand. According to Australian energy statistics, in 2016–17, 63% of the total energy generation was from coal, oil, and natural gas. The energy production from renewable sources (hydro, wind, and solar) increased by 5.3% mainly due to the development of solar and hydro energy which corresponds to 379 PJ, as demonstrated in Fig. 1 (data extracted from Refs. [1]). Renewable energy accounts for 16% of total electricity production and electricity generation from solar, hydro and wind energy increased by 18%, 6%, and 3% respectively [1]. The shutdown of several coal-fired power industries and development in renewable sectors results in the reduction of electricity production from brown coal by 11%.

The geographical location and dry climate with high solar irradiance suggest the potentials for solar power generation. In New South Wales, the 1.1 MW CSP plant with 3500 heliostats is currently under the commissioning phase which will be the first commercially grid-connected CSP plant with thermal storage. Upon successful execution of this project, the 30 MW commercial plant with thermal storage up to 4 h will commence its establishment.

1.3. The superiority of supercritical power cycles

To be a viable dispatchable power generation option, CSP efficiency needs to be increased. The sCO₂ cycles can potentially deliver this improvement. The operating condition of sCO₂ is above the critical condition and exhibits superior thermodynamic properties in the proximity of the critical region [2–5]. Moreover, the sCO₂ has been identified as a chloride-free environmentally safe working fluid with favorable chemical properties (minimum global warming impact with zero ozone depletion potential), thermophysical properties, and lower critical values (31.1 °C and 7.38 MPa) [6–9]. A plethora of research studies highlighted the potential benefits with supercritical CO₂ (sCO₂) Brayton cycle over the conventional steam cycle working under superheated or supercritical conditions [10–14]. The high-fluid density of sCO₂ at the compressor entrance lessens the compression work which subsequently improves the power cycle efficiency [14–16]. The lower specific volume of such working fluid allows a reduction in the physical size of the components and hence a cost reduction. For turbine inlet temperatures above 600 °C, sCO₂ power cycle efficiencies exceed those for He Brayton cycle and steam cycle [17]. In addition, the sCO₂ power cycle can operate under a high range of heat source temperature (600 °C–850 °C and possibly even higher in the future with better materials) for which it is more compatible with the CSP application [14]. More compact heat

exchangers and turbomachinery and simpler plant configuration can reduce the unit capital cost. All of these potential advantages have been well investigated. Dunham and Iverson [11] performed a comprehensive comparison among various power cycles (Carnot, He Brayton cycle, regenerative sCO₂ Brayton cycle, RBC, recompression cycle, RC, combined cycle, RC + ORC, and steam Rankine cycle) for solar tower application and identified sCO₂ recompression cycle, RC, with the maximum thermal efficiency under both dry and wet cooling, as represented in Fig. 2. The cycle maximum temperature for RC is 746 °C and 766 °C under dry and wet cooling and acquiring such higher temperatures are most suited with CSP application.

1.4. Wet vs dry cooling comparison

The best CSP location will have a dry climate with higher solar irradiance. The water resource is scarce in such locations. Even though wet cooling systems deliver a higher cycle efficiency because they dump heat at the wet-bulb temperature instead of the dry bulb, water scarcity makes dry cooling imperative for CSP power plants in arid lands. Dry cooling avoids some environmental challenges associated with wet coolers (water loss due to evaporation, blowdown loss, corrosion, dissolved solids, scale deposition and unwanted and unexpected accumulation of sediments), but entail an efficiency loss. Dunham and Iverson [11] results suggest this efficiency loss is relatively small and even with dry cooling, power tower sCO₂ cycles are still more efficient than the other alternatives. For the sCO₂ RC in Fig. 2, the compressor inlet temperature was assumed to be 53 °C and 32 °C, respectively, for dry and wet cooling. The recompression cycle shows excellent thermal performance in comparison with the steam cycle from 600 °C under wet cooling and 700 °C under dry cooling, as portrayed in Fig. 3. The

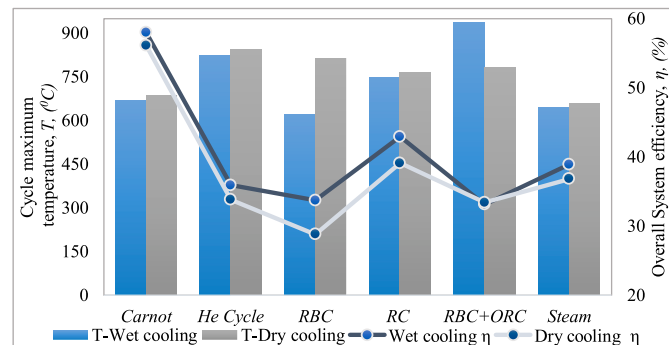


Fig. 2. Cycle comparison under wet and dry cooling. (Data extracted from Ref. [11]).

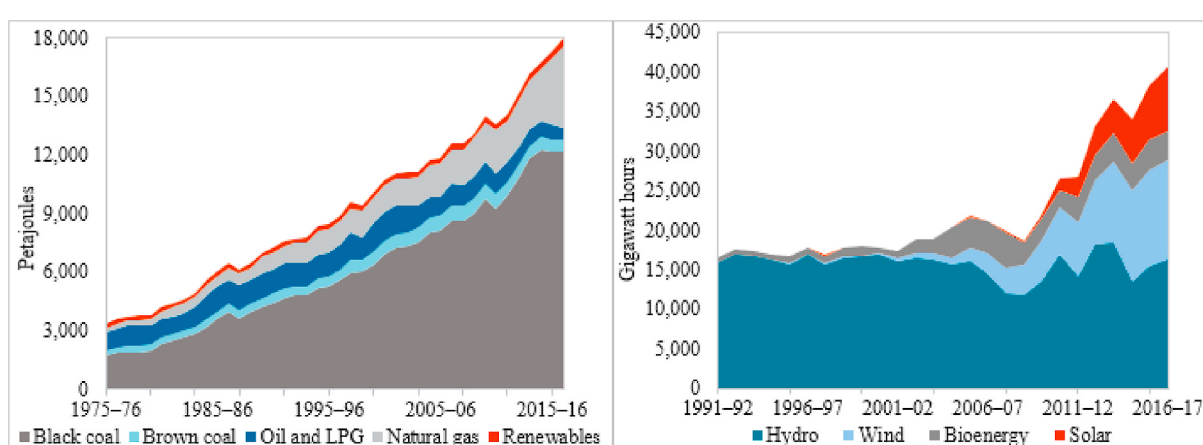


Fig. 1. Energy generation in Australia by fuel type from 1975 to 2016 (left) and from renewable sources (right) from 1991 to 2017. (1 PJ = 278 Gigawatt-hours).

efficiency with dry cooled recompression cycle is comparable against the wet cooled other power cycles at higher heat source temperature.

Conboy et al. [18] investigated the performance comparison of recompression cycle and steam Rankine cycle in the nuclear reactor application. They found dry cooled sCO₂ cycle thermal efficiency to be higher even at hot climate conditions. This is because, unlike a steam Rankine cycle, the supercritical CO₂ cycle designer has another degree of freedom: the cycle low pressure. To enjoy equivalent thermal efficiencies at higher compressor inlet temperatures at high ambient temperatures, the cycle lower pressure can be raised accordingly. Table 1, demonstrates the air cooler design and performance analysis for both cycles under dry and wet cooling conditions.

Another noteworthy observation concerned the relative ease of cooling supercritical CO₂. In steam Rankine cycles, the condensers are subjected to a pinch point restriction due to the process fluid steam condensing at a constant temperature. In a sCO₂ cycle, there is no condensation and the cooling profiles of the process fluid and the cooling fluid are almost parallel implying reduced exergy loss. The steam Rankine cycle requires a six times higher airflow rate for this reason. The higher air mass flow for stream certainly increases the parasitic loss in the cooling tower. The study suggested the ease of cooling with sCO₂ by ambient air in a dry cooler. The performance of dry-cooled sCO₂ cycle was compared against the steam cycle under dry and wet cooling conditions. The authors found that this resulted in a lower cooling system cost for the dry cooler for a sCO₂ power cycle compared with the steam cycle. Besides, for the identical turbine inlet temperature of 550 °C and same cooling duty of 500 MW, higher net power and efficiency acquired with the RC cycle. This study has identified the future commercial prospects for dry cooled sCO₂ power. Zeygami and Khalili [19], Hoo et al. [20], Milani et al. [21], Luu et al. [22], and Son and Lee [23] worked with various layouts of sCO₂ power cycles using dry cooling and confirmed the accomplishment of higher cycle efficiency at higher compressor inlet temperatures.

1.5. Dry cooling system classification

The broad classification of the different cooling system employed in various thermal power plant and process industries is demonstrated in Fig. 4 and a brief description of dry cooling systems are discussed in the following subsections.

In a direct dry cooling system, the hot sCO₂ from the turbine

Table 1

Air cooler design for the same cooling duty and thermal performance analysis of RC cycle and Rankine cycle under dry cooling and wet cooling.

| Design of air cooler | RC Cycle | Rankine cycle |
|-----------------------------------|-------------------------|-------------------------|
| Parameter | | |
| Cooling duty | 500 MW | 500 MW |
| Mass flow rate of cycle fluid | 212 kg/s | 4740 kg/s |
| Air flow rate | 8020 kg/s | 49,470 kg/s |
| Overall thermal conductance, UA | 5.8x10 ⁷ W/K | 5.8x10 ⁷ W/K |
| Inlet temperature | 118.5 °C | 55 °C |
| Outlet temperature | 50 °C | 55 °C |
| The rise of air temperature | 60 °C | 10 °C |
| System performance comparison | | |
| Parameter | RC Cycle | Rankine cycle |
| | Dry-cooled | Dry-cooled |
| Gross power | 333 MW | 250 MW |
| Cycle lowest temperature | 50 °C | 55 °C |
| Cycle maximum temperature | 550 °C | 550 °C |
| Overall system efficiency | 43% | 32% |
| | | Wet-cooled |

* Data extracted from Refs. [18].

discharge is sent to the recuperator where it transfers certain amount of sensible heat to the compressor outlet stream [24] as shown in Fig. 5. The recuperator low-pressure output is then cooled by air inside the cooling tower. Ambient condition significantly impacts on the cooling tower performance [25]. In an indirect cooling system, the outlet low-pressure stream of recuperator is cooled by water in a precooler. The hot water from the precooler then passes through the tubes in the cooling tower and is cooled down with ambient air [26]. Compared with direct cooling, this cooling system requires an additional heat exchanger, the precooler. Although sCO₂ is cooled by water, it is not referred to as "wet cooling". There is no water evaporation loss or blowout loss because the water flows through a secondary circuit and never comes in direct contact with air.

1.6. Dry cooling with CSP technology

The sCO₂ power block integrated with dry cooling technology is well-suited for CSP application not only due to its superior thermal efficiency at identical climate temperature over the traditional steam cycle but also due to the unavailability of adequate water supply in desert areas. The ease of operation and economic merits of using sCO₂ as

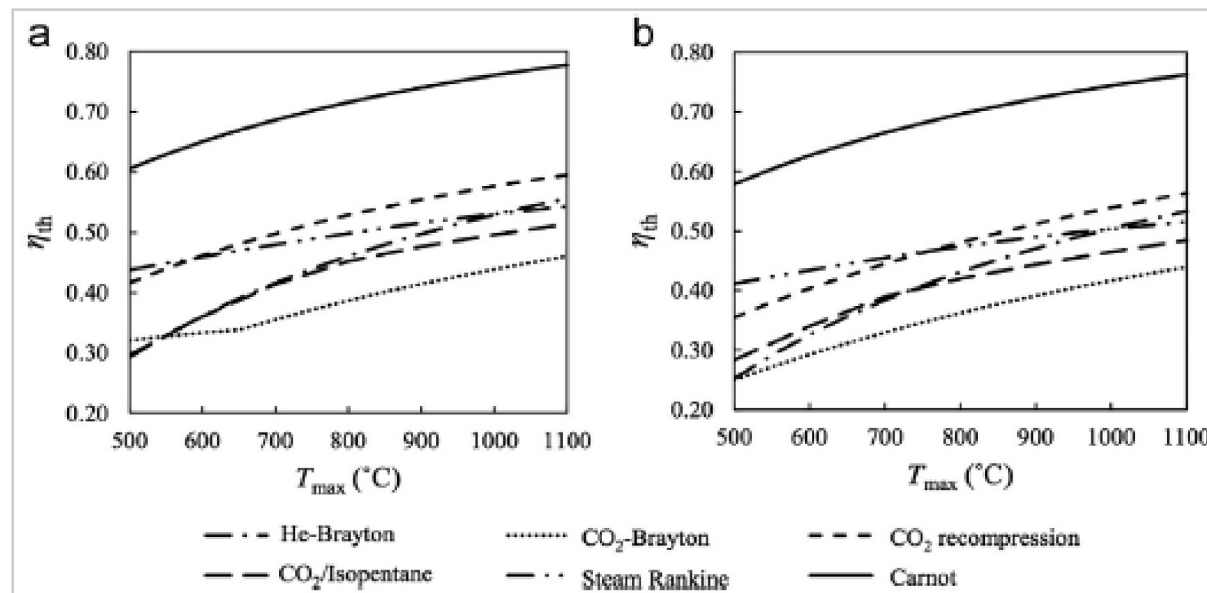


Fig. 3. Cycle performance comparison with (a) wet cooling and (b) dry cooling by Dunham and Iverson [11].

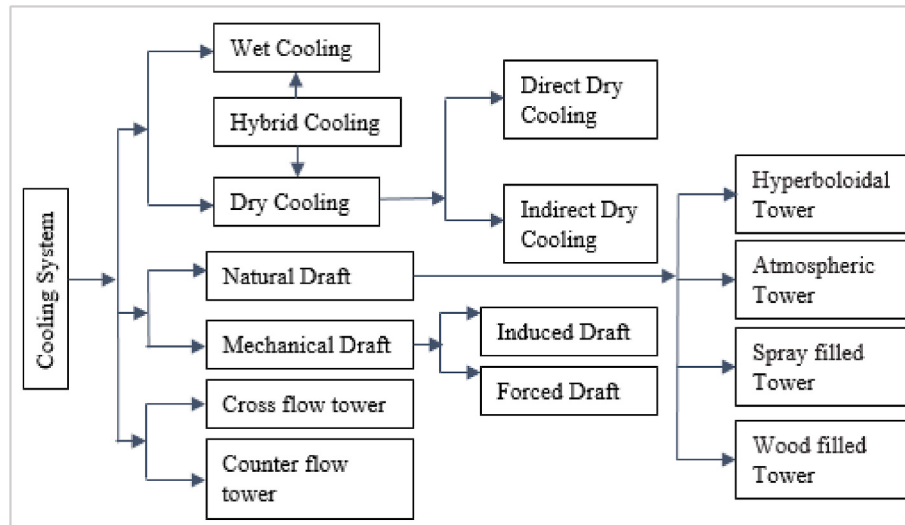


Fig. 4. Classification of cooling system used in the various process and thermal industries.

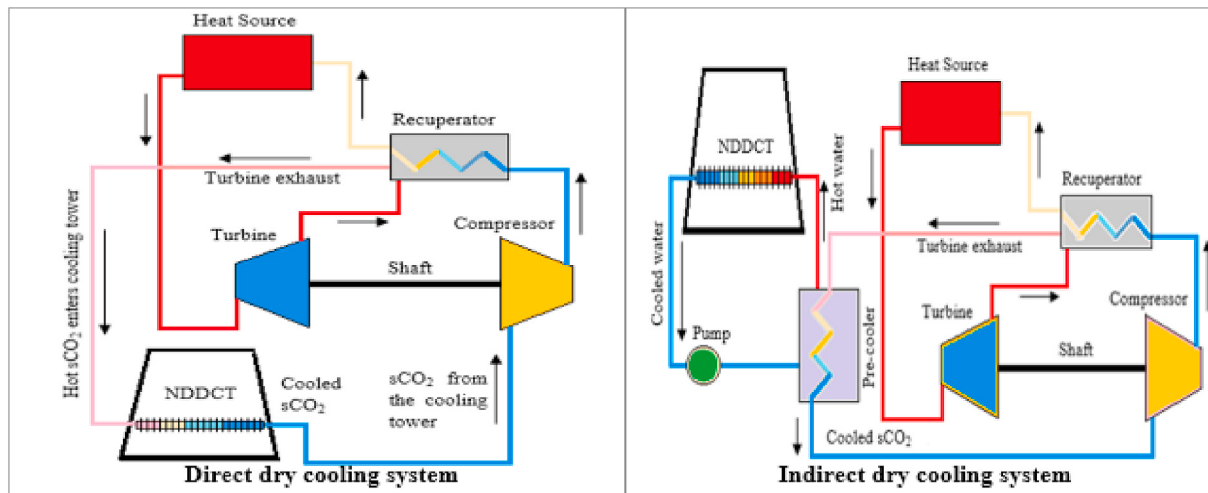


Fig. 5. Recuperative $s\text{CO}_2$ power block coupled with the NDDCT.

working fluid over the conventional steam cycle in dry cooling towers are discussed in Refs. [18]. Padilla et al. [27,28] employed a simple model of air condenser to investigate the thermo-exergetic assessment of different $s\text{CO}_2$ power blocks in the central receiver application. The influence of turbine inlet temperature on the CSP plant efficiency was investigated with five different $s\text{CO}_2$ power cycle layouts followed by detailed exergy analysis [29]. Finned tube air coolers were also considered with various $s\text{CO}_2$ power cycles in CSP technology to perform a comprehensive thermo-economic analysis. The dynamic attributes of the $s\text{CO}_2$ power plant with double stage intercooling and reheating integrated with the solar tower are reported by Osorio et al. [30]. The operational control strategies of a dry cooled CSP plant is investigated with a four-phase dynamic model [22]. Recently, a combined cycle ($s\text{CO}_2$ recompression + LiBr absorption chiller) study is proposed for air-cooled CSP technology [31]. The feasibility of various novel solar salts is studied with recompression cycle coupled with central receiver and performance compared for both dry and wet cooling systems [32]. Ehsan et al. [33] provided detailed cooling tower specifications for $s\text{CO}_2$ power cycles applicable for CSP plant. Later, the power block integrated with a central receiver and thermal energy storage to investigate the year-long performance variation at variant climate conditions [34]. The off-design performance of dry cooled CSP

plant with various heat exchanger design is elaborately studied in Refs. [35].

2. Research status and scopes

2.1. Earlier review

Various possible layouts for $s\text{CO}_2$ power cycles were reviewed for the solar, nuclear reactor, coal-fired, and waste heat applications [36]. Operational characteristics of twelve different $s\text{CO}_2$ power cycles were discussed and their performance in terms of efficiency and recuperator thermal conductance were compared. Experimental test facilities with their operating condition at parts of the world were tabulated [37]. Past studies were not limited to the supercritical region. Kumar and Srinivasan [38] and Sarkar [39] reported the thermodynamic characteristics of CO_2 power cycles under subcritical, transcritical, and supercritical conditions. Mixing CO_2 with various saturated hydrocarbons to modify the critical properties of the working fluid was also reviewed. Crespi et al. [40] performed an extensive review of forty-two different configurations of $s\text{CO}_2$ power cycles highlighting their range of operation, limitation, and advantages over one to another, and the cycles were categorized based on same criteria. Li et al. [41] highlighted potential

implementation in nuclear, solar energy, geothermal, waste heat, and fuel cell applications by reviewing modelling studies, experimental facilities, and equipment readiness. Heat transfer issues with sCO₂ in heating and cooling and the use of thermal compression to lessen the compression work were highlighted. The selection of appropriate heat transfer correlations is important in designing efficient sCO₂ heat exchangers. The influence of various factors (operating pressure, mass flow, tube diameter, wall temperature and buoyancy effect) on the sCO₂ cooling mechanism and heat transfer deterioration under heating mode were comprehensively reviewed [6]. Numerous review studies were performed on proposed heat transfer correlations for sCO₂ in different tube geometries [42–49]. Vignarooban et al. [50] reported the applicability of various molten salts, liquid metals, gas, thermal oil, and organic fluid as a working fluid in the central receiver of the CSP plant driving a sCO₂ power block.

2.2. Present work

The sCO₂ power cycle has all the credentials for long-awaited future generation electricity production. The earlier review works emphasized various aspects of this promising power cycle in different applications. These review works extensively focussed on the diverse layouts of power plant, power cycle classification, the superiority of sCO₂ power cycle over other cycles, cycle optimization, modelling studies, experimental facilities with operational control strategies, development of heat transfer correlation during cooling and heating, design of heat exchangers and recuperators, and present research status on the development of turbo-machineries.

The earlier discussion suggests the eminent suitability of dry cooling in sCO₂ power cycle, particularly for CSP application based on a limited number of case studies. The potential benefits include smoother cooling profile, ease of operation, lower airflow requirement which corresponds to less parasitic losses, maintaining high cycle efficiency during hot climate, and no environmental concerns usually associated with wet cooling. Nevertheless, not one review to date has been performed on the general applicability of dry cooling in the sCO₂ power cycle. Hence the present work exclusively focuses on the feasibility of dry cooling in solar power applications. Aspects of dry cooling with its thermodynamic modelling are discussed. The working principles of the natural draft and mechanical draft cooling towers are demonstrated. A comprehensive summary of past dry cooling studies with sCO₂ power cycles is provided. To provide context to these reviews, dry cooling tower specifications for two promising layouts of sCO₂ power cycle are evaluated based on a detailed modelling approach adapted from Ref. [51]. The cost analysis

- (iii) Section 5, illustrates a case study in which the required cooling system cost and specification for sCO₂ power cycles are presented with a detailed modelling approach.
- (iv) Section 6, represents the design recommendation for future dry-cooled CSP plants.

The ultimate aim of this review paper is to identify the potential benefits of dry cooling technology applied on sCO₂ power block integrated with CSP technology. The detailed methodology of designing such dry cooling towers working under supercritical conditions is prescribed. Various techniques to compensate for the performance degradation associated with sCO₂ dry cooling at extreme climate conditions are recommended. Based on the prescribed methodology, the dry cooling systems are designed with two different sCO₂ power blocks complemented with a thermo-economic comparison.

3. Modelling of a dry cooler

This section provides the fundamental operating principles and key equations for dry cooling systems employing natural and mechanical draft towers.

3.1. Natural draft dry cooling tower

The buoyancy force is produced due to the density difference between the hot inside air and cold outside air. The Natural Draft Dry Cooling Tower (NDDCT) works like a chimney to drive the ambient air across the pipes of the heat exchangers, as shown in Fig. 6. The magnitude of airflow potentially influences by the tower height and the pressure difference. The distorted airflow pattern at the inlet of NDDCT due to tower supports, the flow separation, and the frictional losses while flowing across the heat exchanger potentially impairs the heat exchange process. All these airflow resistances must be considered in the process of evaluation of the draft equation. The cooling potential of a NDDCT depends on the features of the finned tube heat exchanger, the supports, the tower geometry, the tower supports, base of the tower, air temperature, atmospheric pressure, and wind conditions. Comprehensive and fundamental understandings are required for thermally efficient and smooth operation of dry cooling towers. NDDCTs are advantageous and beneficial in comparison with mechanical draft cooling towers due to less energy consumption, simplicity, easier operation, inspection, and maintenance. The operating airflow rate is based on the balance between the chimney effect and the frictional losses through the so-called draft equation.

$$p_{a1} - \left[p_{a5} + \frac{\left(\frac{M_a}{A_5} \right)^2}{2\rho_{a5}} \right] = (K_{is} + K_{ct} + K_{hes} + K_{ctc} + K_{he} + K_{cte}) \frac{\left(\frac{M_a}{A_{fr}} \right)^2}{2\rho_{a34}} + p_{a1} \left[1 - \left\{ 1 - 0.00975 \frac{(H_3 + H_4)}{2T_{a1}} \right\}^{3.5} \right] + p_{a4} \left[1 - \left\{ 1 - 0.00975 \left(H_5 - \frac{H_3}{2} - \frac{H_4}{2} \right) T_{a4} \right\}^{3.5} \right] \quad (1)$$

of the cooling tower is performed for the prescribed cycles.

- (i) Section 3, demonstrates dry cooling system modelling (with natural and mechanical draft) including cooling tower cost models.
- (ii) Section 4, examines various dry cooling studies from the literature summarises key findings from selected research studies. Various cooling techniques adopted in different studies are comprehensively reported.

Various numbers listed in the figure demonstrate the states at different parts of NDDCT. At state 1, ambient air enters the tower and after experiencing tower support loss, the state is now changed to 2. Due to flow redirection and heat exchanger supports the air encounters further losses at state 3. The ACHE bundles contribute the major portion of the total loss due to frictional resistance, contraction, and expansion losses. From state 4 to state 5, the dynamic loss is experienced by the hot air coming out of ACHE bundles. Equations for air properties at different locations of the tower can be found in Ref. [51]. Table 2 lists the

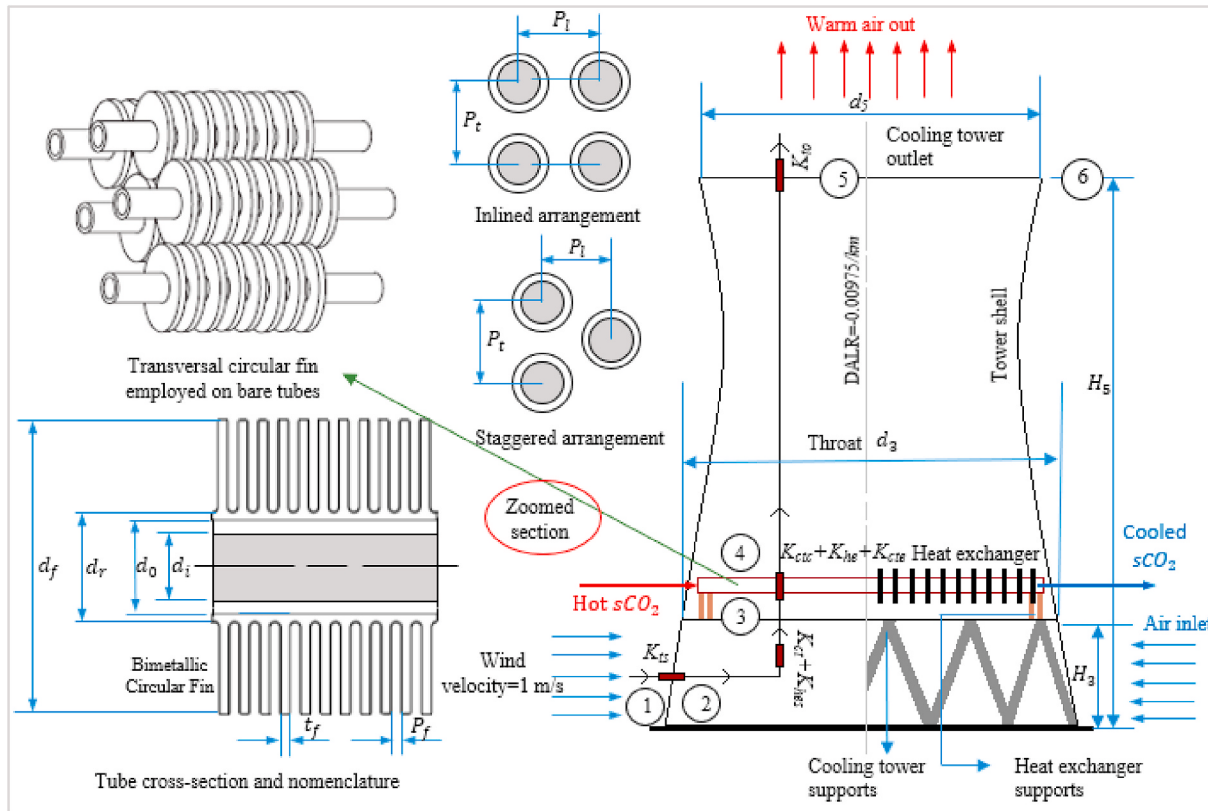


Fig. 6. Details of NDDCT where the heat exchanger tubes are organized in staggered/inlined configurations.

correlations to evaluate the losses. The air heat transfer and friction factor correlations relevant for circular fins are reviewed in Table 3 and Table 4, respectively. Each correlation has its limit of applicability.

3.2. Mechanical draft cooling tower

In this cooling system, the exhaust from the turbine is directed to the finned tube heat exchangers where air flows at a higher volume flow rate utilizing mechanical fans to achieve the required cooling, as shown in Fig. 7. The numbers at different states of the tower represent the airside change of properties due to flow restriction from heat exchanger supports, tower supports, and ACHE bundles. The airside pressure and temperature at each of these states are determined from loss coefficient

3.2.1. Forced draft tower

In a forced draft tower, the fan is installed at the tower base. This produces higher inlet air velocities and lower exit velocities. There are less noise and vibration. Being located at the base, fans are easier to maintain. The heat exchanger bundles can be 2–3 m wide and the finned tubes range from 19 to 51 mm in diameter. Most finned tubes have 350–450 fins/m and may be made of aluminum, copper, steel, stainless steel, or galvanized steel. A typical bay is made up of one or more heat exchanger bundles cooled by two or more axial or propeller type fans; plenum; tower support; heat exchanger support; and other equipment. The bundles can be laid out horizontal or in V's. To prevent the recirculation of warm air exiting the heat exchanger, a wind wall of height H_w is installed. The draft equation is expressed as,

$$\begin{aligned}
 p_{a1} - p_{a7} = & p_{a1} \left[1 - \left(1 - 0.00975 \frac{H_6}{T_{a1}} \right)^{3.5} \right] + K_{ts} \frac{M_a}{A_2} \left(\frac{M_a}{A_2} \right)^2 / 2\rho_{a2} + K_{Fsi} \frac{M_a}{A_c} \left(\frac{M_a}{A_c} \right)^2 / 2\rho_{a3} + K_{up} \frac{M_a}{A_3} \left(\frac{M_a}{A_3} \right)^2 / 2\rho_{a3} \\
 & - \left[\Delta p_{fs} + \alpha_{ef} \frac{M_a}{A_c} \left(\frac{M_a}{A_c} \right)^2 / 2\rho_{a4} \right] + K_{pl} \left(\frac{M_a}{A_c} \right)^2 / \left(2\rho_{a4} \right) + K_{do} \frac{M_a}{A_4} \left(\frac{M_a}{A_4} \right)^2 / 2\rho_{a4} + K_{he} \frac{M_a}{A_{fr}} \left(\frac{M_a}{A_{fr}} \right)^2 / 2\rho_{a56} + p_{a6} \left[1 - \left(1 - 0.00975 \frac{H_7 - H_6}{T_{a1}} \right)^{3.5} \right] \\
 & + \alpha_{e7} \left(\frac{M_a}{A_{fr}} \right)^2 / \left(2\rho_{a7} \right)
 \end{aligned} \tag{2}$$

correlations to estimate the draft force and air flow rate inside the tower. The details calculation of draft force for these towers is elucidated in Refs. [51]. Both axial and centrifugal types of fans are employed in mechanical draft cooling towers. A large amount of power is consumed by fans.

Here K_{Fsi} is fan shroud inlet loss coefficient, A_c and A_h are the casing cross-sectional area and hub cross-sectional area, K_{up} and K_{do} are the upstream and downstream loss coefficient. All other terms and the

Table 2

Correlations to evaluate the various losses in NDDCT.

| Parameter | Equation |
|--|--|
| Tower support coefficient K_{ts} [51] | $K_{ts} = \frac{2\Delta p_{ats}\rho_{a34}}{\left(\frac{M_a}{A_f}\right)^2} = \frac{C_{Dts}L_{ts}d_{ts}n_{ts}A_{fr}^2}{\left(\pi d_3 H_3\right)^3} \left(\frac{\rho_{a34}}{\rho_{a1}}\right)$ $\Delta p_{ats} = \frac{\rho_{a1}v_{a2}^2 C_{Dts} L_{ts} d_{ts} n_{ts}}{2p_{a1} d_3 H_3}; C_{Dts} = 2F_{Dts}/(\rho_{a1} v_{a2}^2 A_{ts})$ <p>Here, L_{ts}, d_{ts}, n_{ts}, and C_{Dts} are support length, effective tower width, number of supports, and support drag coefficient, respectively. A_{ts} and A_{fr} are the areas of tower supports and frontal area of heat exchangers respectively.</p> |
| Contraction coefficient, K_{ctc} [51] | $K_{ctc} = 1 - \frac{2}{\sigma_c} + \frac{1}{\sigma_c^2} \left(\frac{\rho_{a34}}{\rho_{a1}}\right) \left(\frac{A_{fr}}{A_{e3}}\right)^2$ <p>Here, A_{e3} is the area covered by the heat exchangers at the tower inlet.</p> |
| Expansion coefficient, K_{cte} [51] | $K_{cte} = \left(1 - \frac{A_{e3}}{A_3}\right) \left(1 - \frac{A_{e3}}{A_3}\right)^2 \left(\frac{\rho_{a34}}{\rho_{a1}}\right) \left(\frac{A_{fr}}{A_{e3}}\right)^2$ |
| Cooling tower inlet coefficient, K_{ct} | $K_{cthe} = K_{ct} (\rho_{a34}/\rho_{a1}) (A_{fr}/A_{e3})^2$ <p>Terblanche and Kroger [52] correlation,</p> $K_{ct} = \left[100 - 18\left(\frac{d_3}{H_3}\right) + 0.94\left(\frac{d_3}{H_3}\right)^2\right] x K_{he}^{\left[-1.28+0.183\left(\frac{d_3}{H_3}\right)-7.769\times10^{-3}\left(\frac{d_3}{H_3}\right)^2\right]}$ <p>Applicability: $10 \leq \frac{d_3}{H_3} \leq 15$, $5 \leq K_{he} \leq 25$ and $\frac{t_s}{d_3} = 0.005$</p> <p>Preez and Kroger [53] proposed the following,</p> $K_{ct} = \left[-18.6 + 8.1\left(\frac{d_3}{H_3}\right) - 1.084\left(\frac{d_3}{H_3}\right)^2 + 0.0575\left(\frac{d_3}{H_3}\right)^3\right] x K_{he}^{\left[0.165-0.035\left(\frac{d_3}{H_3}\right)\right]}$ <p>Applicability: $5 \leq \frac{d_3}{H_3} \leq 15$, $19 \leq K_{he} \leq 50$</p> <p>Geldenhuys and Kroger [54] reported,</p> $K_{ct} = 0.072\left(\frac{d_3}{H_3}\right)^2 - 0.34\left(\frac{d_3}{H_3}\right) + 1.7$ <p>Preez and Kroger [55] correlation,</p> $K_{ct} = \left[1.04 - 0.009\left(\frac{d_3}{H_3}\right)\right] \left[1.6 - 0.29\left(\frac{d_3}{H_3}\right) + 0.072\left(\frac{d_3}{H_3}\right)^2\right] / s_c + (0.271 - 0.0115K_{he} + 0.000124K_{he}^2)\left(\frac{d_3}{H_3}\right)\left(1.66 - 6.325s_c + 5.625s_c^2\right)$ <p>Applicability: $5 \leq \frac{d_3}{H_3} \leq 10$, $19 \leq K_{he} \leq 50$ and $0.4 \leq s_c \leq 1$</p> <p>Vauzanges and Ribier [56] correlation,</p> $K_{ct} = 1.5 \exp\left(0.2 \frac{d_3}{H_3}\right) K_{he}^{-0.4645+0.02303\frac{d_3}{H_3}-0.00095\left(\frac{d_3}{H_3}\right)^2}$ <p>Applicability: $10 \leq \frac{d_3}{H_3} \leq 15$ and $5 \leq K_{he} \leq 25$</p> <p>Heat exchanger coefficient, K_{he} [51]</p> $K_{he} = \frac{2\Delta p_t}{\rho_{a34}v_{a34}^2} + \frac{2}{\sigma^2} \left(\frac{\rho_{a3} - \rho_{a4}}{\rho_{a3} + \rho_{a4}}\right) + \frac{2\rho_{a4}\left(\frac{1}{\sin\theta_m} - 1\right)}{\rho_{a3} + \rho_{a4}} \left[\left(\frac{1}{\sin\theta_m}\right) + 2K_c^{0.5}\right] + \frac{2\rho_{a4}K_d}{\rho_{a3} + \rho_{a4}}$ <p>K_c and K_d are the inlet and downstream loss coefficients respectively.</p> $\theta_m = 0.0019\theta^2 + 0.9133\theta - 3.1558$ $K_d = \exp[5.488405 - 0.2131209\theta + 3.533265\times10^{-3}\theta^2 - 0.2901016\times10^{-4}\theta^3]$ |
| Tower outlet coefficient K_{to} [51] | $K_{to} = -0.28Fr_D^{-1} + 0.04Fr_D^{1.5}$ $Fr_D = \left(\frac{M_a}{A_5}\right)^2 / [\rho_{a5}(\rho_{a6} - \rho_{a5})gd_5]$ <p>Applicability: $0.5 \leq \frac{d_5}{d_3} \leq 0.85$ and $5 \leq K_{he} \leq 40$</p> |

complete nomenclature can be found in Ref. [51]. The disadvantages associated with forced draft mechanical towers are a non-uniform distribution of air to the heat exchanger and greater possibilities of hot air recirculation due to lower exit velocities.

3.2.2. Induced draft tower

In the induced draft cooling tower, the fan is installed at the tower outlet. Axial or propeller types of fans are employed. Both counter-flow and cross-flow configurations are possible whereas mechanical draft

tower uses a counterflow arrangement. In most thermal and processing industries, induced draft towers are employed due to a better distribution of air and lesser hot air circulation. However, higher fan power is needed and inspection and maintenance are harder as the fans are located at elevation. The higher power consumption is usually outweighed by avoidance of hot air recirculation and better regulation and distribution of air. The draft equation for an induced draft tower is expressed by the following equation.

Table 3

Review of air-side heat transfer correlations.

| Literature | Correlation | Range of applicability |
|----------------------------|--|---|
| Briggs and Young [57] | $\frac{hd_r}{k} = 0.134Pr^{0.33}Re^{0.681} \left[\frac{2(P_f - t_f)}{d_f - d_r} \right]^{0.2} \left(\frac{P_f - t_f}{t_f} \right)^{0.1134}$ <p>Where $Re = \frac{G_a d_r}{\mu_a}$</p> | $1000 < Re < 18000$ $11.013 < d_r < 40.8$ $1.42 < (d_f d_r)/2 < 16.57$ $0.33 < t_f < 2.02$ $1.30 < P_f < 4.06$ $24.49 < P_t < 111$ |
| Vampola [58] | $\frac{hd_e}{k} = 0.251Re^{0.67} \left[\left(\frac{P_t - d_r}{d_r} \right)^{-0.2} \left(\frac{P_t - d_r}{P_f - t_f} + 1 \right)^{-0.2} \left(\frac{P_t - d_r}{P_d - d_r} \right)^{0.4} \right]$ <p>The diagonal pitch is given by</p> $P_d = \frac{P_t}{2} \left(\frac{P_t}{2} \right)^2 \left(\frac{P_t}{2} + P_l^2 \right)^{0.5}, Re = \frac{G_a d_e}{\mu_a}$ $d_e = \frac{A_r d_r + A_f \left(\frac{A_f}{2n_f} \right)^{0.5}}{A_f + A_r}$ | $1000 < Re < 10000$ $10.67 < d_r < 26.01$ $5.20 < (d_f d_r)/2 < 9.70$ $0.25 < t_f < 0.70$ $2.28 < P_f < 5.92$ $20.32 < P_l < 52.4$ $24.78 < P_t < 49.55$ $16.20 < d_e < 34$ $0.48 < (P_t d_r)/d_r < 1.64$ $4.34 < (P_t d_r)/(P_f t_f) + 1 < 25.2$ $0.45 < (P_t d_r)/(P_d d_r) < 2.50$ |
| Mirkovic [59] | $\frac{hd_{et}}{k} = 0.224Pr^{0.33}Re^{0.662} \left(\frac{P_t - d_r}{d_r} \right)^{0.1}$ $\left(\frac{d_r}{P_l - d_r} \right)^{0.15} \left[\frac{2(P_f - t_f)}{d_f - d_r} \right]^{0.25}$ $Re = \frac{G_a d_{et}}{\mu_a}$ $d_{et} = \frac{A_1}{[\pi(d_f - d_r + P_f)]}$ | $3000 < Re < 56,000$ $25.40 < d_r < 50.80$ $9.53 < (d_f - d_r)/2 < 15.88$ $1.27 < t_f < 2.03$ $4.23 < P_f < 8.47$ $60 < P_t < 80$ $100 < P_t < 120$ |
| Ganguli et al. [60] | $\frac{hd_r}{k} = 0.38Re^{0.6}Pr^{0.333} \left(\frac{A}{A_r} \right)^{-0.15}$ $Re = \frac{G_a d_r}{\mu_a}$ $\frac{A}{A_r} = \frac{(A_f + A_r)}{A_r} = \left[\frac{d_f^2 - d_r^2}{2} + d_f t_f + d_r (P_f - t_f) \right] / (d_r P_f)$ | $11.176 < d_r < 50.8$ $5.842 < (d_f - d_r)/2 < 19.05$ $2.3 < P_f < 3.629$ $0.254 < t_f < 0.559$ $27.432 < P_t < 98.552$ $1800 < Re < 100000$ $1 < (A_f + A_r)/A_r \leq 50$ |
| Rabas et al. [61] | Colburn factor, $j = 0.292Re^n \left(\frac{P_f}{d_r} \right)^{1.12} \left(\frac{P_f}{t_f} \right)^{0.26} \left(\frac{t_f}{P_f} \right)^{0.67} \left(\frac{d_r}{d_o} \right)^{0.47} \left(\frac{d_f}{t_f} \right)^{0.77}$ | Low fin height, small fin spacing, and staggered configuration |
| Wang et al. [62] | $n = -0.415 + 0.0346 \frac{d_r}{P_f}$ $j = 0.394Re^{-0.392} \left(\frac{t_f}{d_r} \right)^{-0.0449} n_r^{-0.0897} \left(\frac{P_f}{d_r} \right)^{-0.197}$ | $300 < Re < 7500$ Staggered configuration |
| Gianolio and Cuti [63] | $h = 0.314 \frac{k}{d_o} Re^{0.681} Pr^{0.333} \left(\frac{P_f}{t_f} \right)^{0.1134} \left(\frac{P_f}{d_r} \right)^{0.2} \left(1 + \frac{v_\infty}{n_r} \right)^{-0.14}$ | Staggered configuration |
| Chi-Chuan Wang et al. [64] | $j = 0.086Re^{0.1} n_r^{0.2} \left(\frac{P_f}{d_f} \right)^{0.3} \left(\frac{P_f}{d_a} \right)^{0.4} \left(\frac{P_f}{P_t} \right)^{0.93}$ $p1 = -0.361 - \frac{0.042n_r}{\log(Re)} + 0.158 \left(n_r \left(\frac{P_f}{d_f} \right)^{0.41} \right)$ $p2 = -1.224 - \frac{0.076 \left(\frac{1.9 - 0.23 \log(Re)}{d_f} \right)^{1.42}}{\log(Re)}$ $p3 = -0.083 + \frac{0.058n_r}{\log(Re)}$ $p4 = -5.735 + 1.211 \log \left(\frac{Re}{n_r} \right)$ | Maximum number of row is 8 Low fin height, small fin spacing and staggered configuration |

$$\begin{aligned}
 & p_{a1} - 0.00975H_7 - H_4 \Bigg) \Bigg/ T_{a4} \Bigg\} \Bigg] (H_7 - H_4)/T_{a4} \Bigg]^{3.5} - \left[1 - 0.00975H_7 - H_4 \right] \Bigg/ T_{a1} \Bigg\} (H_7 - H_4)/T_{a1} \Bigg]^{3.5} = K_{ts} \frac{M_a}{A_2} \left(\frac{M_a}{A_2} \right)^2 \Bigg/ 2\rho_{a1} \Bigg) + K_{ct} \left(\frac{M_a}{A_{fr}} \right)^2 \Bigg/ \left(2\rho_{a1} \right) \\
 & + K_{he} \frac{M_a}{A_{fr}} \left(\frac{M_a}{A_{fr}} \right)^2 \Bigg/ 2\rho_{a34} \Bigg) + K_{pl} \frac{M_a}{A_c} \left(\frac{M_a}{A_c} \right)^2 \Bigg/ 2\rho_{a4} \Bigg) + K_{up} \frac{M_a}{A_e} \left(\frac{M_a}{A_e} \right)^2 \Bigg/ 2\rho_{a4} \Bigg) - K_{fs} + \alpha_{ef} \Bigg) \frac{M_a}{A_c} \left(\frac{M_a}{A_c} \right)^2 \Bigg/ 2\rho_{a4} \Bigg) + K_{do} \frac{M_a}{A_e} \left(\frac{M_a}{A_e} \right)^2 \Bigg/ 2\rho_{a4} \Bigg) \\
 & + K_{dif} \frac{M_a}{A_c} \left(\frac{M_a}{A_c} \right)^2 \Bigg/ 2\rho_{a4} \Bigg) + \alpha_{ef} \left(\frac{M_a}{A_7} \right)^2 \Bigg/ \left(2\rho_{a4} \right)
 \end{aligned} \tag{3}$$

4. Research studies with sCO₂ power cycles using dry cooling

The ability to maintain higher cycle efficiency of sCO₂ cycles during hot and humid weather has been demonstrated [69]. The cycle

performance of various power block layouts (RBC, RC, PC, and MC) integrated with dry cooling were evaluated at compressor inlet temperature of 45 °C and 60 °C. The MC cycle with single-stage reheating showed a maximum efficiency of 52.6% followed by the PC and the RC cycle. The performance also compared against steam Rankine cycle with several feedwater heaters and one reheat and the results showed that

Table 4
Review of airside pressure drop correlations.

| Literature | Correlation | Range of applicability |
|----------------------------|---|--|
| Robinson and Briggs [65] | $Eu = \frac{\rho \Delta P_a}{G_a^2} =$ $18.93n_r Re^{-0.316} \left(\frac{P_t}{d_r} \right)^{-0.927} \left(\frac{P_t}{P_d} \right)^{-0.515}$ $Re = \frac{G_a d_r}{\mu_a}$ $P_d = \frac{P_t}{2} \left(\frac{P_t}{2} \right) \left(\frac{P_t}{2} \right)^2 + P_f^2 \right)^{0.5}$ $f_{RB} = 9.465 Re^{316} \left(\frac{P_t}{d_o} \right)^{-0.927} \left(\frac{P_t}{P_d} \right)^{0.515}$ $f = \frac{1}{2} \frac{d_a}{P_t} f_{RB}$ | $2000 < Re < 50,000$ $18.64 < d_f < 40.89$ $39.68 < d_f < 69.85$ $10.52 < (d_f - d_r)/2 < 14.48$ $42.85 < P_t < 114.3$ $37.11 < P_t < 98.99$ $2.31 < P_f < 2.82$ $1.8 < P_f/d_r < 4.6$ $\text{Low fin height, small fin spacing, and staggered configuration}$ |
| Nir [66] | $f = 1.24 Re^{-0.25} W^{-0.32} \left(\frac{d_f}{d_o} \right)^{-0.25} K_p$ | $\text{Low fin height, small fin spacing, and staggered configuration}$ |
| Jacob [67] | $f = \frac{4}{\pi} \left(0.25 + \left[\frac{0.118}{\left(\frac{P_t}{d_r} - 1 \right)} \right]^{1/08} Re^{-0.16} \right) \left[\left(\frac{P_t}{d_r} \right) - 1 \right]$ | $\text{Low fin height, small fin spacing, and staggered configuration}$ |
| Kim et al. [68] | $f =$ $1.455 Re^{-0.656} \left(\frac{P_t}{P_l} \right)^{-0.347} \left(\frac{P_f}{d_o} \right)^{-0.134} \left(\frac{P_t}{d_r} \right)^{1.23}$ $Eu = \frac{\rho \Delta P_a}{G_a^2} = 0.7315 n_r Re^{-0.245} \left(\frac{P_t - d_r}{d_r} \right)^{-0.9}$ $\left(\frac{P_t - d_r}{P_f - t_f} + 1 \right)^{0.7} \left(\frac{d_a}{d_r} \right)^{0.9}$ $Eu = \frac{\rho \Delta P_a}{G_a^2} =$ | $\text{Low fin height, small fin spacing, and staggered configuration}$ $\text{Same as heat transfer correlation}$ |
| Vampola [58] | $3.96 n_r Re^{-0.31} \left(\frac{P_t - d_r}{d_r} \right)^{-0.14} \left(\frac{d_r}{P_l - d_r} \right)^{0.18}$ $\left[\frac{d_f - d_r}{2(P_f - t_f)} \right]^{0.2}$ $Re = \frac{G_a d_{eh}}{\mu_a}$ $d_{eh} = 4[P_t P_f - \pi(d_f^2 t_f + P_f d_f^2 - d_r^2 t_f)]/A_1$ | $1600 < Re < 31000$ $25.40 < d_r < 50.80$ $9.53 < (d_f - d_r)/2 < 15.88$ $1.27 < t_f < 2.03$ $4.23 < P_f < 8.47$ $60 < P_f < 80$ $100 < P_t < 120$ $\text{Same as heat transfer correlation}$ |
| Mirkovic [59] | $Eu = \frac{\rho \Delta P_a}{G_a^2} = 2n_r \left[1 + \frac{2 \exp \left\{ - \frac{P_t - d_r}{4d_r} \right\}}{\left\{ 1 + \frac{P_t - d_r}{d_r} \right\}} x \left[0.021 + \frac{13.6(d_f - d_r)}{Re(P_f - t_f)} + 0.25246 \left(\frac{(d_f - d_r)}{Re(P_f - t_f)} \right)^{0.2} \right] \right]$ $Re = \frac{G_a d_r}{\mu_a}$ | $300 < Re > 7500$ $\text{Staggered configuration}$ |
| Ganguli et al. [60] | $f =$ $1.039 Re^{-0.418} \left(\frac{t_f}{d_f} \right)^{-0.104} n_r^{-0.0935} \left(\frac{P_f}{d_f} \right)^{-0.197}$ $\text{For } 2 < n_r < 8$ $f = 138.3 Re^{-0.478} \left(\frac{P_t}{d_o} \right)^{-1.454}$ $\text{For } 10 < n_r < 17$ $f = 32.72 Re^{-0.412} \left(\frac{P_f}{d_o} \right)^{-1.54} \left(\frac{A_a}{A_o} \right)^{0.3}$ $f = 0.0267 Re^{f1} \left(\frac{P_t}{P_l} \right)^{f2} \left(\frac{P_f}{d_f} \right)^{f3}$ $f1 = -0.764 + 0.739 \frac{P_t}{P_l} + 0.177 \frac{P_f}{d_f} - \frac{0.00758}{n_r}$ $f2 = -15.689 + \frac{64.021}{\log(Re)}$ $f3 = 1.696 - \frac{15.695}{\log(Re)}$ | $1 < n_r < 7$ $6.35 < d_o < 12.7$ $1.19 < P_f < 8.7$ $17.7 < P_t < 31.75$ $12.4 < P_l < 27.5$ |
| Wang et al. [62] | $f =$ | |
| Gianolio and Cuti [63] | $1.039 Re^{-0.418} \left(\frac{t_f}{d_f} \right)^{-0.104} n_r^{-0.0935} \left(\frac{P_f}{d_f} \right)^{-0.197}$ $\text{For } 2 < n_r < 8$ $f = 138.3 Re^{-0.478} \left(\frac{P_t}{d_o} \right)^{-1.454}$ $\text{For } 10 < n_r < 17$ $f = 32.72 Re^{-0.412} \left(\frac{P_f}{d_o} \right)^{-1.54} \left(\frac{A_a}{A_o} \right)^{0.3}$ $f = 0.0267 Re^{f1} \left(\frac{P_t}{P_l} \right)^{f2} \left(\frac{P_f}{d_f} \right)^{f3}$ $f1 = -0.764 + 0.739 \frac{P_t}{P_l} + 0.177 \frac{P_f}{d_f} - \frac{0.00758}{n_r}$ $f2 = -15.689 + \frac{64.021}{\log(Re)}$ $f3 = 1.696 - \frac{15.695}{\log(Re)}$ | $1 < n_r < 7$ $6.35 < d_o < 12.7$ $1.19 < P_f < 8.7$ $17.7 < P_t < 31.75$ $12.4 < P_l < 27.5$ |
| Chi-Chuan Wang et al. [64] | | |

the sCO₂ power cycle with any layout showed superior performance in comparison with the steam cycle for the compressor inlet temperature ranging from 45 °C to 65 °C. Besarati and Goswami [5] also reported the requirement of more than 50% cycle efficiency with the dry cooled RC cycle. The cycle efficiency was further improved by 3–7% considering an ORC combined with the sCO₂ power cycles to exploit the waste heat. Different organic fluids were employed to optimize the overall cycle efficiency of the combined cycle. The Cis-butene and R245fa were identified as the most efficient working fluids of the ORC cycle combined with the RBC and the PC and RC cycle respectively. Dyreby et al. [70] reported the inherent advantages of dry-cooled sCO₂ cycles over the traditional steam cycle. The closer cooling tower temperature approach is possible between air and sCO₂ in the dry cooling tower since the heat rejection process is not restricted by the saturation temperature of sCO₂. The efficiency drop at high air temperatures could be addressed by increasing the cycle lower pressure, an option not available to the steam power plant operator. Garg et al. [10] employed air cooler to investigate the enhancement of thermal performance of a trans-critical CO₂ cycle over the steam cycle with respect to efficiency, the specific volume of working fluid, and exergy destruction. Moisseytsev and Sienicki [71] worked on the detailed design of shell and tube heat exchanger where sCO₂ flowed inside the tubes and fins employed on the shell side to augment the surface area for the airside. The effect of the fin pitch and the diameter ratio on the heat rejection was investigated. The authors also proposed the design of air-cooled printed circuit heat exchanger and compared heat rejection performance against the finned shell and tube heat exchanger. Hu et al. [72] altered the critical properties of sCO₂ by mixing it with various gas additives with preferred mole fraction as a result, the critical pressure of the working fluid raised which resulted in reduced compression work, and higher efficiency. The dry cooling was assumed while modelling the power cycle for nuclear reactor application. Padilla et al. [27] also considered dry cooler as the heat rejection component and investigated the cycle irreversibility and efficiency performance by the influence of pressure drop in the heat exchanger and solar receiver. The influence of reheating on the cycle performance and exergetic assessment was conducted where the dry cooler and central receiver contributed the majority of the total exergy losses [28]. The RBC, RC, PC, and MC cycles were considered to compare the thermal performance with respect to cycle highest temperature ranging from 500 °C to 850 °C [29]. Ho et al. [20] employed A-frame finned tube heat exchanger unit to assess the tech-economic evaluation of sCO₂ power cycles for CSP application. The cost equations presented for the power cycle components, the heliostat field, the solar receiver, and the thermal energy storage. Ma et al. [73] studied the impact of intercooling in the recompression cycle and presented a mathematical model for the optimization of cycle pressure ratio and split ratio between the compressors. With dry cooling (cycle minimum temperature of 50 °C) employed, the efficiency improved by 1.23% and 1.65% by the main compression intercooling over the reference condition for a cycle highest temperature of 500 °C and 800 °C respectively. Li et al. [74] experimented with trans-critical CO₂ cycle to explore the impact of thermal oil mass flow rate in the heat source and CO₂ mass flow rate on the thermal performance. Fan assisted finned tube air cooler was used as the heat rejection component and the control strategies of the experimental rig were demonstrated. Ma et al. [31] proposed an economic assessment of a novel dry cooled sCO₂ power cycle (RBC combined with absorption chiller) integrated with molten salt solar power tower and reported an efficiency improvement of 5.19% over the RBC cycle. The influence of pressure drop in the heat exchanger and air temperature fluctuation on the cycle performance was also investigated. Pidaparti et al. [75] developed a mathematical model for the induced draft wet cooling tower where water absorbed the heat from the hot working fluid in the pre-cooler and then chilled by ambient air in the cooling tower. The water mass flow rate and inlet temperature were optimized for economic operation of the power plant and results showed the amount of water savings against the direct water-cooling method.

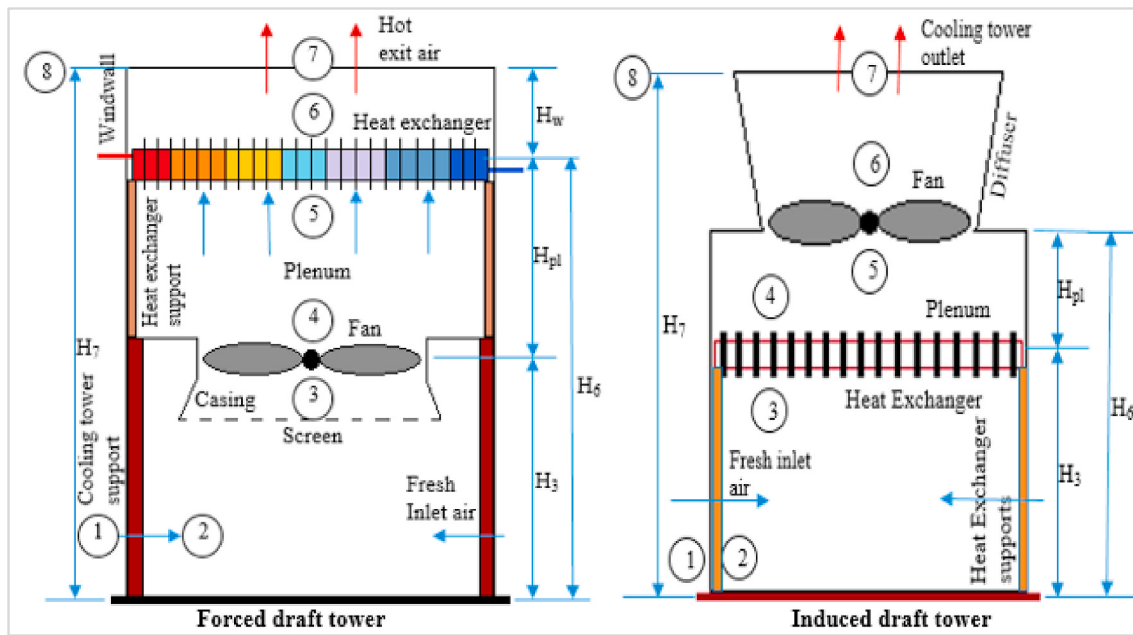


Fig. 7. The schematics of mechanical draft towers where the various states of air are numbered to reflect the draft equation for each case.

The above discussion on dry-cooled sCO₂ power cycles mostly focused on cycle thermal performance and system optimization at various operating conditions. Air-cooler design methodologies specific to a sCO₂ cycle were generally ignored in most of these studies with a few exceptions. Table 5, outlines the key findings of the studies with dry-cooled sCO₂ power cycles from the existing literature. Only a few studies (Singh et al. [76,77], Dunham and Iverson [11], Zeyghami and Khalili [19], Milani et al. [21], Duniam et al. [25], and Ehsan et al. [24,78,79]) are identified with a focus on the cooling performance of the sCO₂ power cycles and are discussed in the following subsections. These studies are important to evaluate the feasibility of dry cooling in CSP plants.

4.1. Dynamic modelling with dry cooler

Singh et al. [76] investigated the dynamic performance of a 1 MW solar-assisted recuperated Brayton cycle by controlling the mass inventory with an extremum seeking controller (ESC) to optimize the plant performance at various seasonal conditions. The higher solar irradiation in the summer season resulted in a rise in turbine inlet temperature from the design condition (350 °C) due to the decrease of sCO₂ mass flow consequential to higher air temperature and lower specific heat of sCO₂ in the heat source. Conversely, in winter the low ambient temperature overcooled the cycle beyond the design condition at compressor inlet (32 °C), and the system operated under a subcritical state in the low-pressure side of the power cycle. Depending on the solar input and ambient temperature at a given amount of time, the adaptive ESC continuously evaluated the plant performance and changed the CO₂ mass inventory at the compressor inlet to operate the cycle near the design condition at the turbine inlet and optimize the cycle thermal performance. The ESC approach also successfully implemented for power optimization and system stabilization in fuel cell [84], solar photovoltaics [85], water chiller [86], and wind turbine [87]. Fig. 8, shows the modelling of a solar assisted sCO₂ cycle equipped with the cooling tower. The solar system is a parabolic-trough collector in which the sCO₂ directly heated by the solar component and eliminated the usage of an additional intermediate heat exchanger. The design point parameters of the cycle and the methodology of modelling of heat exchangers, turbine, and compressor described elaborately in Ref. [77]. A proportional-integral controller employed in the cooling tower to regulate the air mass flow rate during the winter season. The controller

also regulated the air temperature thus ensuring a supercritical state of working fluid at the compressor inlet. The performance of ESC compared against the fixed inventory approach in which during summer, the excessive increase of turbine inlet temperature was addressed by increasing the sCO₂ mass inventory from 300 kg/m³ to 382 kg/m³.

Fig. 9 demonstrates the system dynamic response with respect to the varying solar input and ambient temperature on a typical summer day. Early in the day during high solar irradiation, the ESC controlled the turbine inlet temperature and pressure in the proximity of the prescribed design condition. The net power dropped significantly for the period when solar heat input is low for both control schemes. Superior performance obtained with the ESC approach in comparison with the fixed inventory approach. The similar response obtained during the winter season; however additional airflow controller used in the cooling tower to maintain the air temperature at a point for which the working fluid retained its supercritical state in the compressor inlet.

Osorio et al. [30] performed the transient behavior of a solar-heated dry-cooled regenerative Brayton cycle with two-stage intercooling and reheating. The system optimization performed based on the mass flow, the pressure ratio, and the recuperative area. The influence of variant solar irradiation on the net power generation and system efficiency was performed during various seasonal conditions and the thermal storage with two tanks up to 8 h of capacity reduced the temperature fluctuation at the turbine inlet. Luu et al. [22,88] also presented a dynamic model of a solar-assisted and dry-cooled recompression cycle to investigate the startup operation with four successive phases and control strategies to sustain the supercritical state under full load operation.

4.2. Enhancing the cooling potential by radiative cooling

Radiative cooling prior to the compressor was proposed to mitigate the efficiency drop at higher ambient temperature [19]. A radiative cooler properly coated with the selective radiative materials can emit heat in the far-infrared spectrum and absorb short-wave radiation from the sun [89,90]. If the radiative heat flux emitted from the surface surpasses the absorbed solar irradiation, there is a net cooling effect that may be sufficient to compensate for the increased ambient temperature [91,92]. As a result, the temperature of the sCO₂ inside the radiative cooler further decreases which leads to the improvement of cycle efficiency. A radiative cooler absorbs the visible sunlight with a short

Table 5

Review Summary on sCO₂ Brayton cycles equipped with the dry cooling technology.

| Literature | Cycle Configuration | Key Findings | Dry Cooling | Remarks |
|---------------------------|------------------------------------|---|-------------|--|
| Conboy et al. [18] | RBC and RC | Investigation of cycle performance during hot and humid weather conditions | Yes | Finned tube heat exchanger was designed. |
| Hu et al. [72] | RC | Usage of various gaseous additives with pure CO ₂ as a working fluid to alter its critical properties. | Assumed | No details of cooling component |
| Zeyghami and Khalili [19] | RBC and RC | Thermal performance of CSP plants under various ambient temperature and influence of an additional cooling system. | Yes | Radiative dry cooler in addition to forced draft air cooler was used |
| Padilla et al. [27] | RC, PC, and MC | Thermodynamic modelling and exergy analysis of various sCO ₂ cycles by the influence of pressure drop and reheating. | Yes | The air cooler was used but no information on the physical size |
| Padilla et al. [28] | RC | Optimization of recompression cycle and analysis of thermal efficiency and exergy. | Assumed | No details of cooling component |
| Padilla et al. [29] | RC, PC, and MC | Thermal assessment of various cycles for CSP application; Influence of pressure drop and reheating on cycle performance. | Assumed | No details of cooling component |
| Hoo et al. [20] | RC, PC, and MC | Cycle modelling; Thermal performance and economic assessment of power cycles integrated with CSP. | Yes | A-frame, finned tube air cooler was used but not designed |
| Osorio et al. [30] | RC with intercooling and reheating | Cycle modelling; Cycle optimization; Dynamic analysis of sCO ₂ power cycle under various operating conditions. | Yes | The air cooler was used but no information on the physical size |
| Milani et al. [21] | RC with intercooling and reheating | Modelling and optimization of the solar field and various cycle parameters for acquiring the highest thermal efficiency | Yes | The hybrid cooling method was used |
| Li et al. [74] | RBC | An experimental study with a trans-critical CO ₂ power cycle; Demonstration of the system start-up operation, | Yes | The finned tube air-cooled condenser was used with fans |

Table 5 (continued)

| Literature | Cycle Configuration | Key Findings | Dry Cooling | Remarks |
|-------------------------------|-----------------------------|---|-------------|--|
| Luu et al. [22] | RC | normal operation, and control strategies. | | |
| Ma et al. [73] | RC with intercooling | The start-up and control strategies for the sCO ₂ recompression cycle. | Yes | The air cooler was used but not designed |
| Persichilli et al. [4] | RBC | Cycle modelling; study the impact of intercooling on cycle power generation | Assumed | No details of cooling component |
| Singh et al. [76, 77] | RC | Application of Echogen heat engine for waste heat recovery; Benefits of sCO ₂ power cycle over conventional steam | Assumed | No details of cooling component |
| Turchi et al. [69] | RC, PC, and MC | Cycle modelling; Dynamic behavior of the cycle in various seasonal conditions with the variant solar radiation | Assumed | No details of cooling component |
| Besarati and Goswami [5] | RBC, RC, and PC | Study of thermal efficiency of various sCO ₂ cycle layouts with reheat. | Assumed | Proposed for air-cooled heat exchanger |
| Dyreby et al. [70] | RC | Study of cycle performance and implementation of organic Rankine cycle for utilization of exhaust heat. | Assumed | No details of cooling component |
| Garg et al. [10] | RBC | Study of design parameters for optimum cycle performance; Modelling of recuperators by the thermal conductance. | Assumed | No details of cooling component |
| Dunham and Iverson [11] | RBC, RC, and combined cycle | Cycle modelling; A comparative investigation between trans-critical CO ₂ and conventional steam cycle for CSP. | Yes | Air-cooler was used but no information on the physical size |
| Moisseytsev and Sienicki [80] | RC | Thermal assessment of various cycles for CSP application; Thermal and economic analysis of the power cycle. | Assumed | No details of cooling component |
| | | Detailed modelling approach; Feasibility evaluation of dry cooling in the sCO ₂ Brayton cycle over the wet coolers; Performance comparison of air coolers. | Yes | Air-cooled printed circuit heat exchanger and finned shell and tube heat exchanger |

(continued on next page)

Table 5 (continued)

| Literature | Cycle Configuration | Key Findings | Dry Cooling | Remarks |
|-----------------------|---------------------|---|-------------|---|
| Ma et al. [31] | RC | Study the combination of an absorption chiller and recompression Brayton cycle for the waste heat recovery application. | Yes | Air-cooler was used but no information on the physical size |
| Li et al. [41] | RC, PC, and MC | Modelling of power cycles and its applicability in solar, nuclear reactor, and other potential energy sectors. | Assumed | No details of cooling component |
| Neises and Tuchi [14] | RC, PC, and MC | Thermodynamic study of several sCO ₂ power cycles combined with solar tower; Cycle efficiency comparison | Assumed | No details of cooling component |
| Cheng et al. [81] | RC | Optimization of the sCO ₂ power cycle by sensitivity analysis; Cycle maximum pressure and the efficiency of the turbo-machineries were optimized | Assumed | No details of cooling component |
| Son and Lee [23] | RC | Cycle modelling; Optimization of the sCO ₂ power cycle by adjoint sensitivity analysis; Cycle transient response | Yes | Air-cooler was used but no information on the physical size |
| Linares et al. [32] | RC, PC, and MC | CSP plant performance; feasibility of various solar salts; comparison between dry and wet cooling; economic analysis | Assumed | No details of cooling component |
| Wang et al. [35] | RC | Optimizing the heat exchanger design; Thermal performance assessment | Yes | Finned tube heat exchanger was used |
| Ehsan et al. [33,82] | RC and PC | Thermal assessment; cycle comparison; designing dry cooling tower; economic assessment of dry cooling towers | Yes | Detailed modelling of dry cooling tower was used |
| Ehsan et al. [34,83] | RC | Novel power cycle modelling; CSP plant dynamic modelling; annual variation of net power; | Yes | Detailed modelling of dry cooling tower was used |

*RBC-Regenerative Brayton cycle, RC-recompression cycle, PC-Partial cooling cycle, MC-Main Compression with intercooling cycle, and ORC-Organic Rankine cycle.

wavelength and reflects a comparatively higher wavelength to the atmosphere in the range of 8 μm–13 μm known as atmospheric window [93–95]. This atmospheric window is assumed to be placed above the radiative surface and transmittance is high enough in this range [91]. Any downward atmospheric irradiation represents an extremely cold temperature [95,96].

The cooling potential of a radiative cooler is highly dependent on the radiative properties of surface materials [91,97–99]. Such a device is expected to be a lot more effective at night when the plant is producing from storage. Night-time radiative cooler has been successfully experimented by Granqvist and Hjortsberg [92], Catalanotti et al. [93], Al-Nimir et al. [94], Kimball [95], Nilsson and Niklasson [97], Nilsson et al. [99], and Gentle and Smith [100]. However, the development of a well-designed and efficient radiative cooler with lower absorptivity and higher emissivity in the atmospheric window is an active area of research especially during the daytime period when solar irradiation is quite intense. Rephaeli et al. [91] presented a model of daytime radiative cooler made with a dielectric photonic structure which reflected more than 95% solar irradiation with high emissivity in the atmospheric window and produced a cooling heat flux of 100 W/m². Raman et al. [98] experimented with a radiative cooler coated with seven different layers of materials to provide cooling under solar insolatation of 850 W/m² and reflected more than 97% of solar irradiation. The results showed the acquirement of 4.9 °C below atmospheric temperature and produced a cooling heat flux of 40 W/m². Fig. 10 demonstrates the schematic diagram of a radiative cooler. The fundamental equations to model the radiative cooler are comprehensively presented in Ref. [101].

Zeyghami and Khalili [19] performed a preliminary analysis to enhance the cooling potential of a dry-cooled sCO₂ power cycle by the implementation of a radiative cooler prior to the compressor inlet. The RC and the RBC layouts were considered coupled with a central receiver for the system modelling. The key outcome was to determine the required radiative cooler area to obtain the desired cycle minimum temperature. At moderately higher ambient temperature, the additional cooling load was determined from the air cooler to attain the desired compressor inlet temperature with the radiative cooler. The power cycles were modelled with air cooler to provide a cycle minimum temperature of 55 °C at an ambient temperature of 41 °C. The role of the radiative cooler is to reduce the temperature of sCO₂ prior to compressor inlet by 15 °C.

Fig. 11 shows the evaluation of radiative cooling load and the corresponding cooler area for 15 °C temperature reduction prior to the compressor inlet. For 800 °C cycle highest temperature, the cycle performance for RBC enhanced by 3.1% whereas for RBC the improvement was 4.9%. The required radiative cooling load for RC was 138% higher than that of RBC layout due to the higher heat capacity inside the radiative cooler. The total heat rejection duty of the power cycle decreased with the reduction of cycle minimum temperature. The radiative cooling load almost proportionately augmented with the increase of temperature drop and the slope was higher for the RC cycle. For RBC, a radiative cooler of 4.38 m²/kW was required for whereas, for RC, the required surface area increased to 10.46 m²/kW. The air-cooling duty and total cooling load reduced by 18.5% and 5.6% for RBC and 46% and 9.4% for RC respectively. The result showed the potential of a radiative cooler in sCO₂ power cycle; however, the variation of solar irradiation and fluctuation of ambient temperature were not considered. Besides, the detailed design methodology of a radiative cooler was not mentioned. Hence, further developmental efforts are required to evaluate the feasibility of a radiative cooler in the sCO₂ power cycle under variant solar irradiation and ambient temperature.

4.3. Performance enhancement by hybrid cooling

The present article highly emphasizes the application of dry cooling for CSP application working with a sCO₂ power cycle. The hybrid cooling approach can address the adverse impact of dry cooling in terms

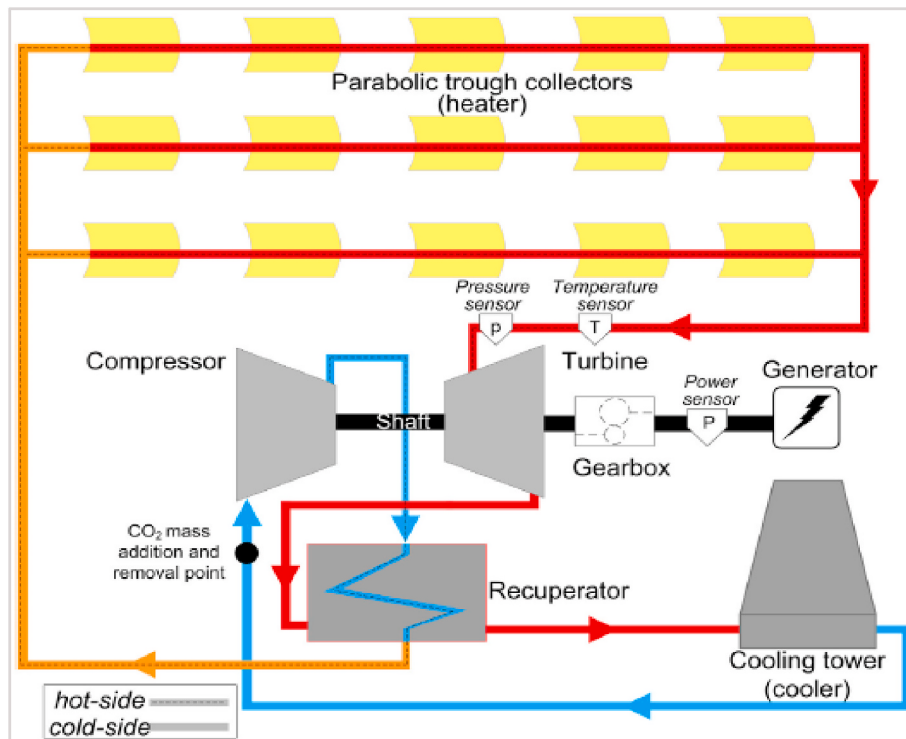


Fig. 8. Solar assisted recuperated sCO₂ cycle integrated with the dry heat dissipation system [76].

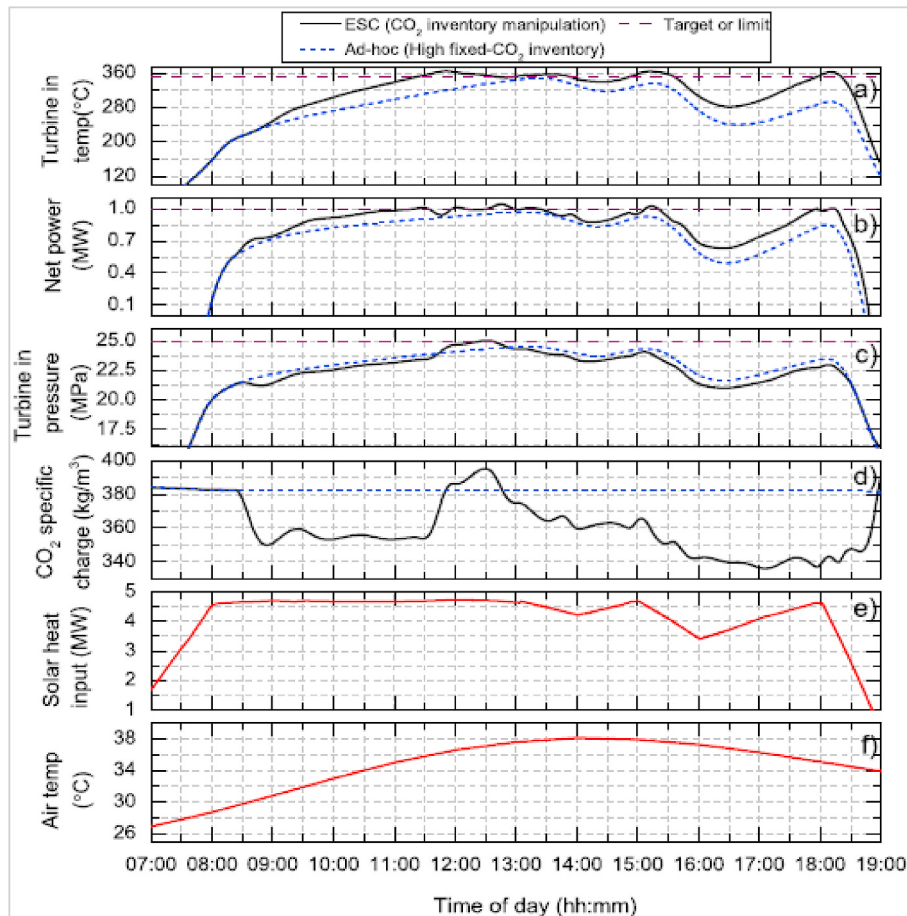


Fig. 9. Dynamic response of sCO₂ power cycle with ESC during summer season [76].

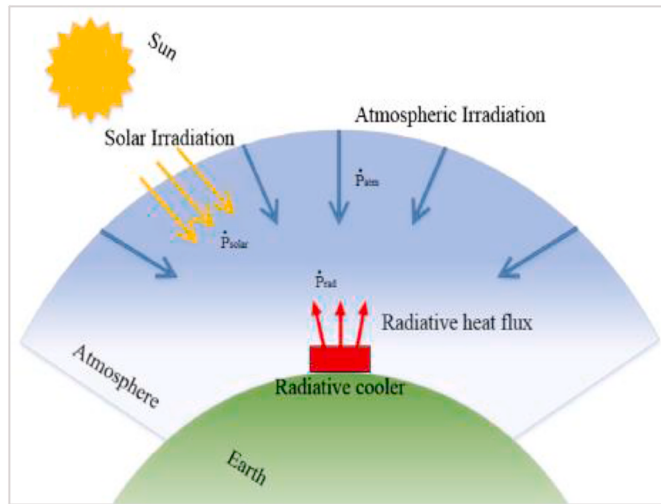


Fig. 10. Heat balance of a radiative cooler [19].

of efficiency degradation and lower net power generation, especially during the hot climate. Wagner and Kutscher [102] performed a dynamic simulation with the steam cycle integrated with the central receiver to assess the water-saving of 52% by hybrid cooling over the dry cooling. Barigozzi et al. [103,104] performed a system optimization to maximize the net power generation of a steam cycle in the waste heat energy application. The optimum cooling strategy of using dry mode/hybrid mode in different climate conditions was demonstrated. Rezaei et al. [105] reported the dynamic operation of a hybrid cooling tower (wet cooling tower and air-cooled condenser) to lessen the water consumption using series and parallel configuration. Sadafi et al. [106,107] enhanced the cooling performance by suggesting the use of saline water to precool the inlet air by spraying prior to the entrance of heat exchanger in the inlet of a cooling tower. The complex mechanism of droplet formation, evaporation, trajectory, and potential advantages of using saline water over freshwater were outlined. Alkhedhair et al. [108–110] performed experimentation and modelling study to explore the dynamics of spray assisted cooling mechanism in NDDCT. The inlet air precooled by 8.1 °C and the influence of wind velocity, humidity ratio, spray dispersion on the cooling performance was demonstrated. Goodarzi and Keimanesh [111] improved the cooling performance by employing a radiator type windbreaker under cross-wind condition. Zou et al. [112–114] worked with an innovative hybrid cooling tower in

which the solar chimney combined with NDDCT to improve cooling effectiveness and produce power and dissipate waste heat simultaneously to operate a geothermal power plant. Ghorbani et al. [115] integrated the solar chimney into a dry cooler to augment the thermal efficiency by 0.5% of a steam Rankine cycle.

The available literature on hybrid cooling mostly applied for steam Rankine cycle. Milani et al. [21] analyzed the cycle performance of fourteen different sCO₂ layouts based on three key performance indicators (cycle efficiency, heat exchanger area, and cooling duty). The combined cycle (recompression cycle with single-stage intercooling and reheating) selected as the best candidate for integration with the central receiver. The sCO₂ was directly heated in the solar tower which eliminated the usage of an additional heat exchanger. The thermal storage was not considered to economize the capital cost of the solar field and additional fossil fuel energy source employed to lessen the fluctuation of solar irradiation at the turbine inlet. The cooling arrangement of the power cycle configured in two different mechanisms (wet cooling and hybrid cooling). In the wet cooling method, two water coolers employed for the 1st and 2nd stage of compression, whereas for the hybrid cooling method, a pair of water cooler and air cooler employed for each stage of compression which in turn required total four coolers in a hybrid case. Depending on the ambient condition, the hybrid cooling operated under three distinct modes (air only mode, air-water mix mode, and water only mode). The water coolers in both cases used in a closed-loop and dry cooling tower used to precool water by ambient air. The heat exchanger area and the physical size of the forced draft air cooler were reported

Table 6
The cooling mechanism of sCO₂ during the first stage and final stage.

| Parameter | First stage | Final Stage |
|---|----------------------------------|------------------------------------|
| Cooler physical size | 10.6x13.3x0.26 (m ³) | 10.6x15.48x0.278 (m ³) |
| Heat exchange area | 19,082 m ² | 17,615 m ² |
| Cooling duty | 0.57 MW | 0.48 MW |
| sCO ₂ mass flow | 49.9 kg/s | 49.9 kg/s |
| Air flow rate | 468 kg/s | 672 kg/s |
| Air inlet and outlet temperature | 25 °C and 36.1 °C | 25 °C and 31.5 °C |
| sCO ₂ inlet and outlet temperature | 68.3 °C and 32.2 °C | 37 °C and 31.9 °C |
| Water inlet and outlet temperature | 30 °C and 36 °C | 30 °C and 36 °C |
| Air cooling mode | 70% | 63% |
| Water cooling mode | 0% | 5% |
| Air-water mix mode | 29% | 31% |
| Failure to cool below 32 °C | 1% | 1% |

*Data extracted from Refs. [21].

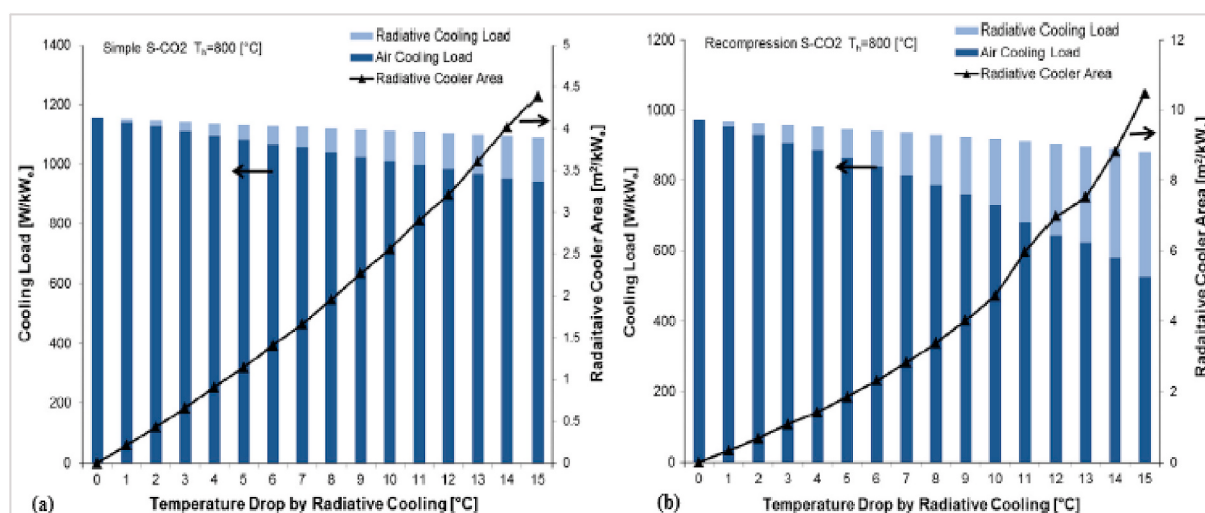


Fig. 11. Evaluation of cooling load and cooler area for 15 °C decrement for (a) RBC and (b) RC cycle [19].

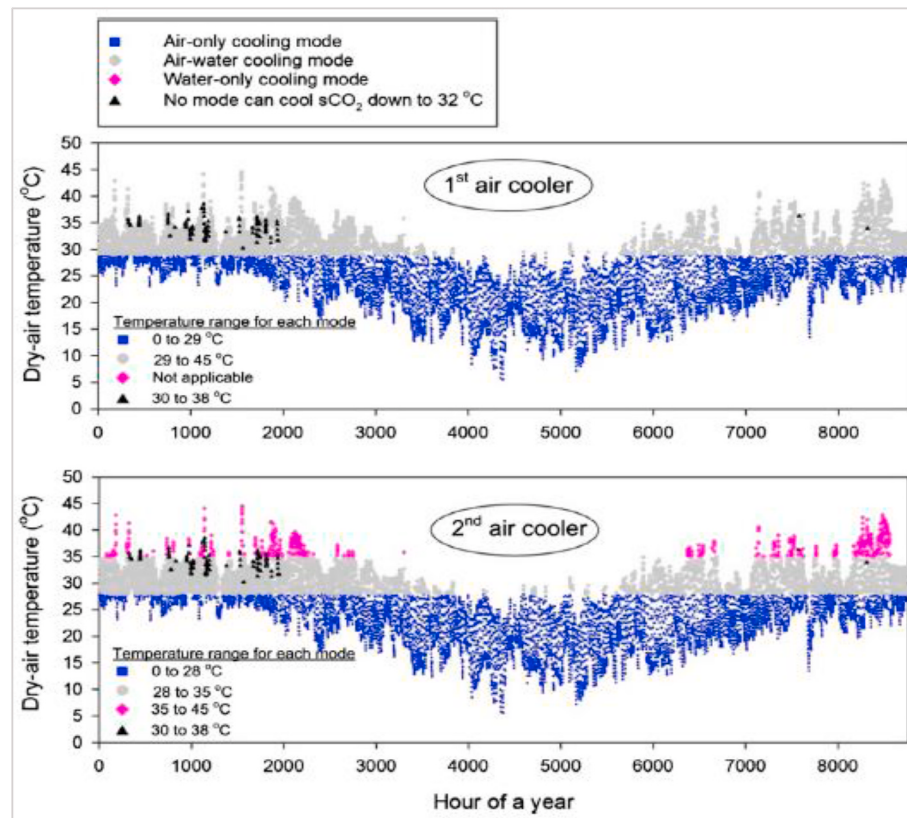


Fig. 12. The hybrid cooling mechanism in the air coolers of a solar-powered recompression cycle with single-stage reheating and intercooling [21].

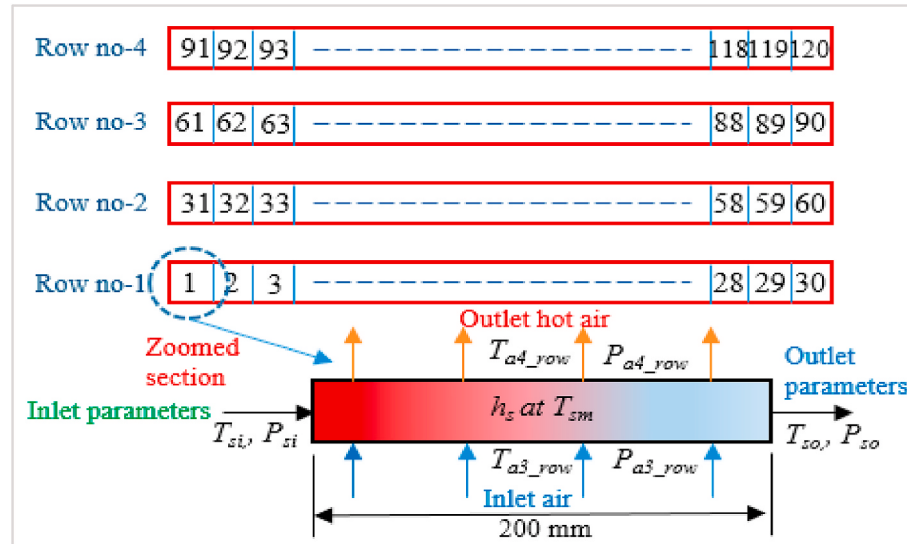


Fig. 13. The nodal method used in the heat exchanger inside NDDCT [78].

using ASPEN, as shown in Table 6. The air cooler designed for an ambient temperature of 25 °C and the design point compressor inlet temperature set at 32 °C. Depending on the ambient air temperature (0 °C–29 °C), the fan power increased by 150% to reduce the sCO₂ temperature within the target of 32–32.5 °C. The shortage of cooling demand not fulfilled by the air only mode was performed by air-water mix only mode when the air temperature was in the range of 29 °C–45 °C, as shown in Fig. 12. The water only mode was not initiated during the 1st stage of cooling since the sCO₂ entered the cooling system at a higher temperature of 68.3 °C. During the 2nd cooling stage, the inlet

temperature of sCO₂ reduced to 37 °C which increased the water consumption to acquire the desired outlet temperature. The air-only mode and air-water mix mode applied for the air temperature in the range of 0 °C–35 °C. For both cooling stages, the working fluid was not cooled to 32 °C even with the water only cooling mode due to the violation of pinch point in the cooling tower during hot and humid climate conditions (wet bulb temperature more than 28 °C). The higher initial temperature between air and sCO₂ during the first cooling stage required the air only cooling mode operating 70% of the time and the control system shifted towards the air-water mix mode during the 2nd cooling stage.

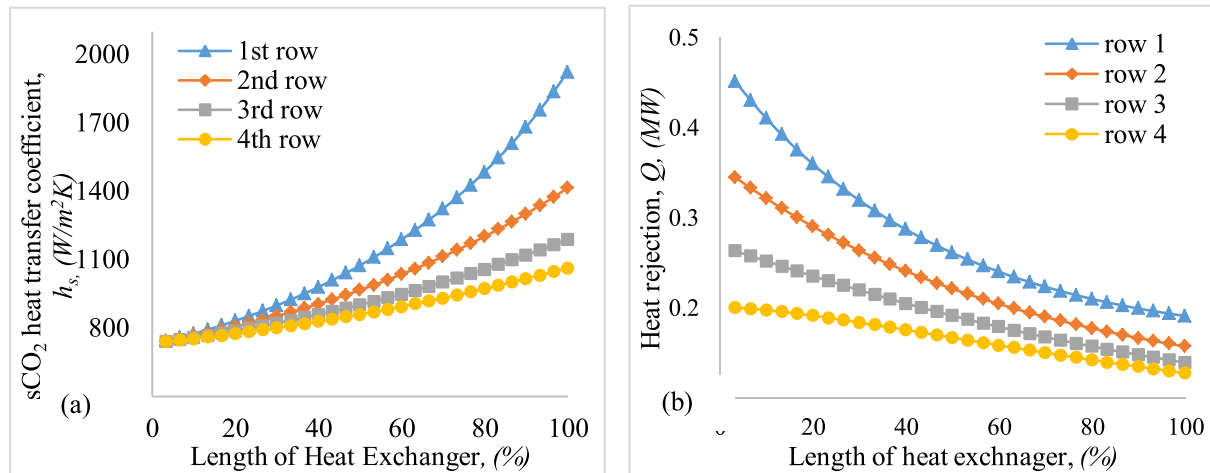


Fig. 14. Local variation h_s and Q in the heat exchanger [78].

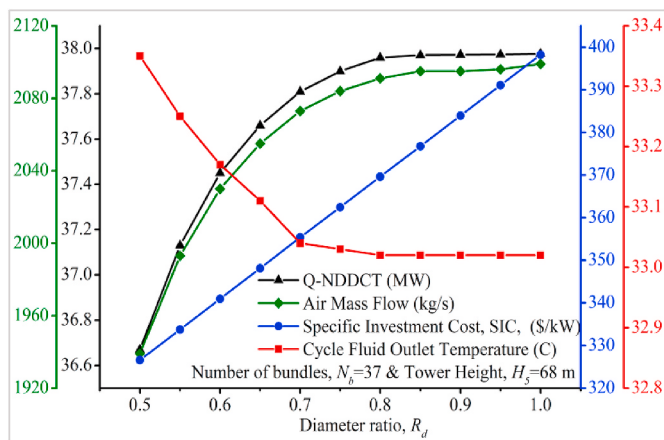


Fig. 15. Optimizing the diameter ratio of NDDCT integrated with RC cycle [82].

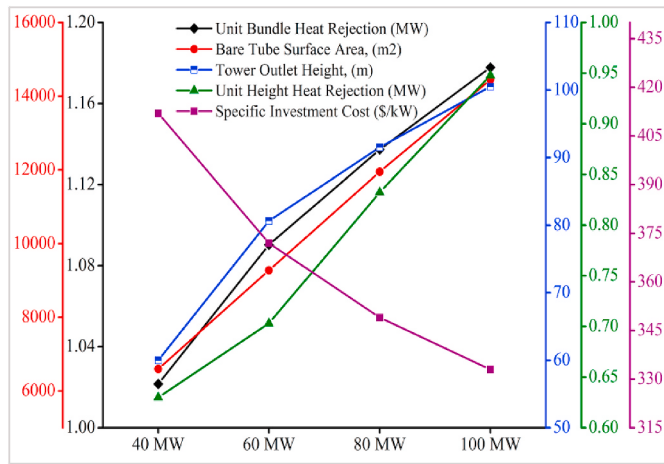


Fig. 16. Designing NDDCT for several capacities of RC power cycle [82].

The results of hybrid cooling compared against the wet cooling method to observe the water savings in terms of levelized water consumption (L/MWh). Approximately 80% of water savings acquired with the hybrid cooling method. One noteworthy observation of this study is operating the cycle with a fixed $s\text{CO}_2$ inlet temperature at variant

ambient air conditions. It is expected that during a hot and humid climate, the inlet temperature of $s\text{CO}_2$ also increases [25]. Hence, it is required to perform the power cycle simulation with a hybrid cooling approach considering the change of the inlet temperature of $s\text{CO}_2$ in the cooling tower.

4.4. Detailed NDDCT modelling approach

A plethora of articles analyzing the assessment of $s\text{CO}_2$ cycles using dry cooling considered the cooling system as a black box with the desired compressor inlet temperature. Ehsan et al. [24,78] presented a detailed NDDCT model working with supercritical CO_2 for direct and indirect cooling systems. The validated one-dimensional MATLAB code with the nodal technique applied in the heat exchanger allowed the determination of property changes for both $s\text{CO}_2$ and airside, as shown in Fig. 13. The air properties, pre-cooler inlet conditions, and fixed geometric ratios of cooling tower adapted from Kroger's one-dimensional model [51] provided as inputs. The program started the calculation with a fixed heat exchanger bundles and initial estimates of outlet temperatures. Next, the code calculates the airside and $s\text{CO}_2$ side properties, tower geometries, and surface areas of heat exchanger bundles. The NDDCT model evaluated the draft equation by measuring the airflow resistance at different positions of the tower. Once the draft equation was solved, the code then checked the temperature crossover across the tube length and the outlet temperature of $s\text{CO}_2$. The code changed the initial estimates in order to acquire the design point outlet temperature of $s\text{CO}_2$. After accomplishing the duty requirements, the code provided the specification of the required cooling system.

Fig. 14 demonstrates the variation of h_s and Q in the single-tube pass heat exchanger. At the tube inlet, the $s\text{CO}_2$ bulk temperature was higher and gradually decreased by the ambient air. The tube side heat transfer coefficient increased at the end of the tube as the bulk temperature approached to pseudocritical temperature. For the rest of the row of tubes, the h_s variation was less due to increased $s\text{CO}_2$ temperature and an increase in air temperature. The higher initial temperature difference led to higher heat transfer at the inlet of the tube. The Q value gradually decreased and similar performance reported for the other row of tubes. Ehsan et al. [116] recently conducted the exergy analysis of a recompression cycle with a comprehensive modelling approach adapted in cooling tower. Ehsan et al. also [79,83] investigated the impact of climate variation on the NDDCT equipped $s\text{CO}_2$ power cycle for CSP application. Recompression cycle was considered for optimizing the geometry of NDDCT followed by a comprehensive economic assessment of cooling tower. The NDDCT aspect ratio and diameter ratio were optimized based on specific investment cost (SIC) and the desired outlet temperature of the tower, as demonstrated in Fig. 15. The diameter ratio

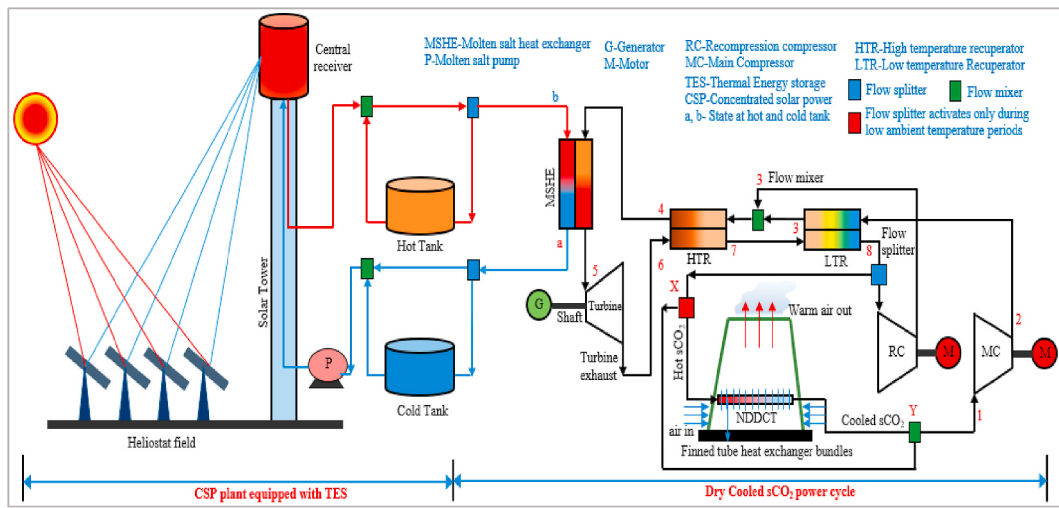


Fig. 17. NDDCT equipped with RC power block and CSP technology [34].

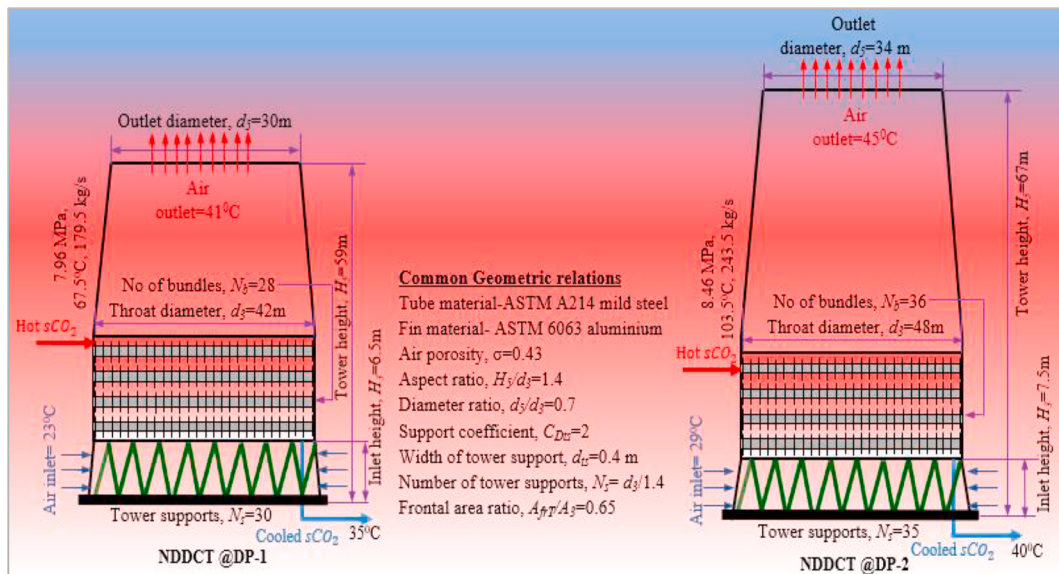


Fig. 18. Measurement of NDDCT for two design conditions of a CSP plant [34].

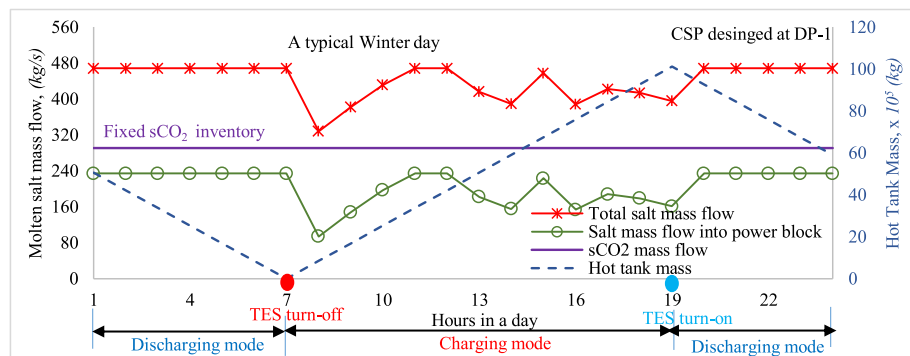


Fig. 19. TES operation in a typical winter day of a dry-cooled CSP plant [34].

optimized at 0.7 beyond which SIC increased significantly. The NDDCT outlet shape was convergent in shape which ruled out the possibility of cold-inflow at the outlet of NDDCT and reduced the dynamic loss. In Fig. 16, the required sizing of NDDCT evaluated for higher capacities of

net power generation. The unit bundle heat rejection and unit height heat rejection both increased for higher capacities, however, SIC found to be minimum for lower power generation. The paper also comprehensively reported the cost assessment of NDDCT with optimized

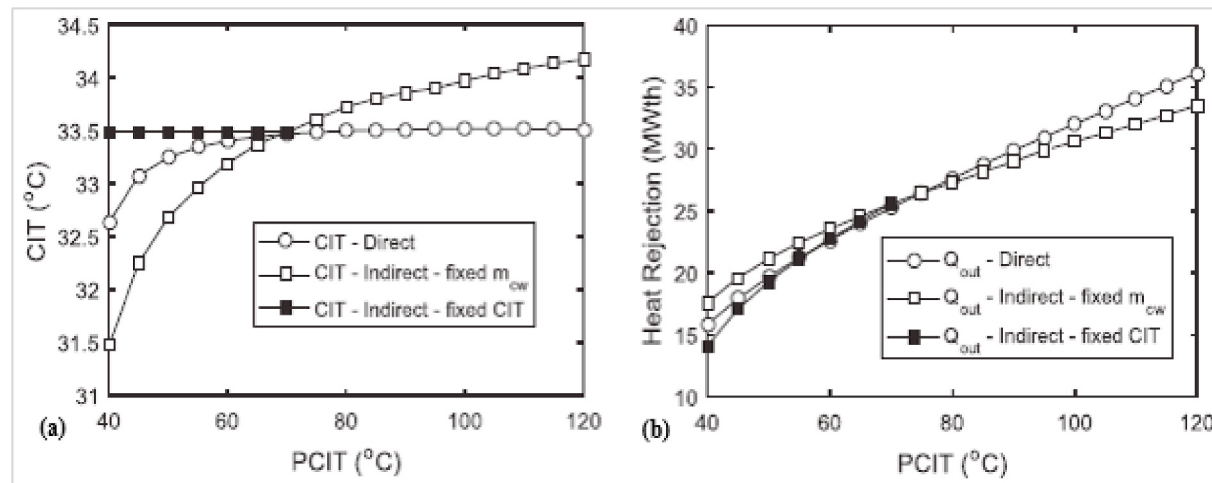


Fig. 20. Cooling system comparison with respect to PCIT variation [25].

geometry.

Later, this sCO₂ power block with optimized NDDCT geometry integrated with a central receiver and thermal energy storage (TES) and CSP plant annual performance was investigated for variant seasonal climates [34], as demonstrated in Fig. 17. The various design parameters of power block (mass flow, pressure ratio, and NDDCT outlet temperature) and central receiver (solar salt temperatures, mass flow, and TES capacity) were optimized before integrating it with NDDCT. The thermal performance of a CSP power plant operated with the sCO₂ power cycle is

highly influenced by the variant nature of climate conditions. Hence, the NDDCT was designed considering two air temperature based on average climate temperature and maximum frequency in a specific CSP location. Fig. 18 reveals the sizing of NDDCT designed against air temperature 23 °C and 29 °C respectively. It is noted that the choice of design point (DP) climate temperature also influenced the desired NDDCT outlet temperature or main compressor outlet temperature and pressure ratio. For higher air temperature case, the requirement of sCO₂ mass flow and compressor outlet pressure is higher for the accomplishment of the same

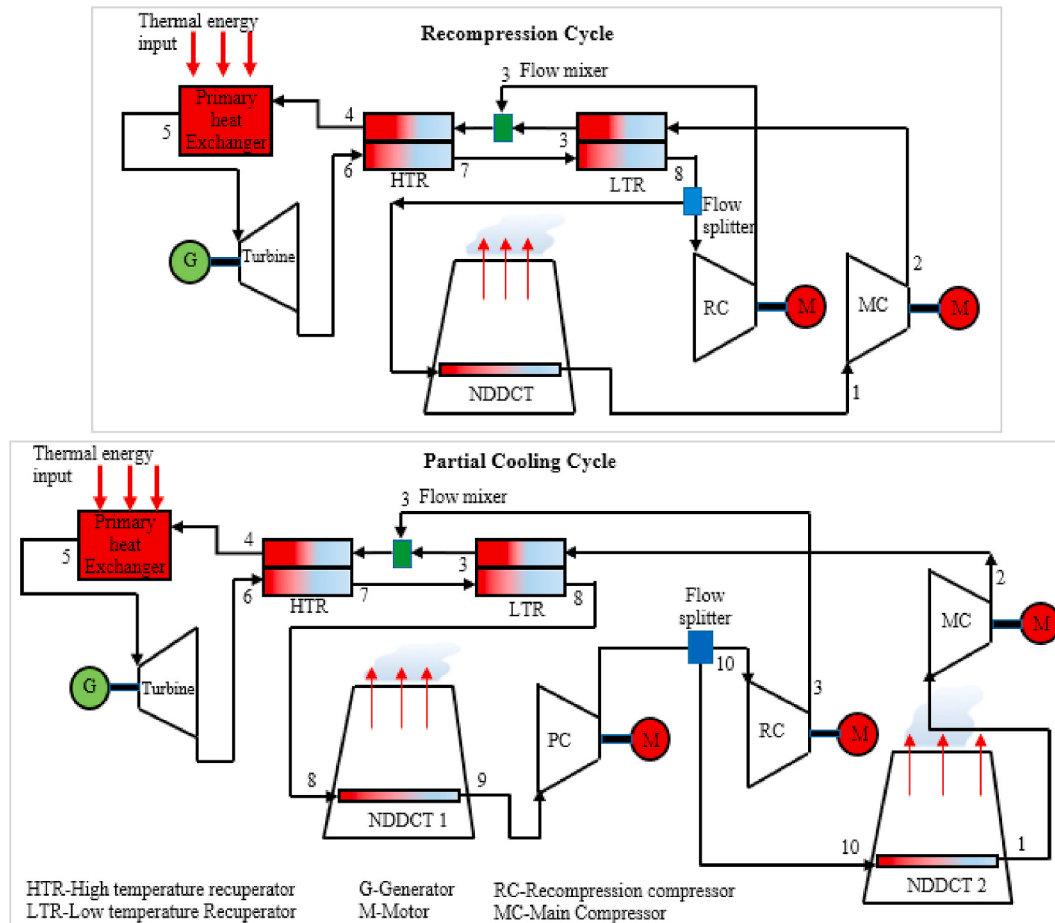


Fig. 21. Tower modelling for recompression and partial cooling cycle.

work output. This consequently required a higher tower height in comparison with lower climate temperature. During the winter season, the cycle overcooling was prevented by employing additional flow splitter prior to NDDCT whose function was to bypass an amount of mass so that the cycle always operated under supercritical conditions. This supplementary flow splitter provided operational stability by reducing the heat rejection in NDDCT during extreme winter conditions. Fig. 19 reveals the TES dynamic operation on a typical winter day. During nighttime when the cycle operated under TES heat input, the net power generation remained stable. Nevertheless, during daytime under the fluctuation of solar irradiance and climate temperature, the variation in power generation was significant. The variant climate condition during the daytime also required adjusting the solar salt mass flow and cycle fluid mass flow for optimized plant operation.

Duniam et al. [25] performed a coupled analysis of recompression SCO_2 cycle with NDDCT to model the tower and compare the thermal performance of the direct and indirect system. The direct system for a 25 MW power generation required a tower height of 55.9 m in comparison with 71.6 m for the indirect system and 40% less heat exchanger area for the accomplishment of the same cooling duty. The higher inlet temperature of the working fluid into NDDCT required a tower height with a lower elevation. The cycle efficiency compared for a range of ambient temperature (0 °C–50 °C) and sCO_2 inlet temperature (40 °C–120 °C) into NDDCT. At a climate temperature of 50 °C, the efficiency dropped to 44.7% and 43.8% for direct and indirect respectively. For an indirect cooling system, the cooling water mass flow rate was optimized for the various operating condition. The better thermal performance with the direct system at higher ambient temperature also confirmed by Ehsan et al. [24].

The cooling tower designed for both cooling systems at pre-cooler inlet temperature (PCIT) of 71 °C. Any PCIT below the design point, overcooled the cycle with lower compressor inlet temperature (CIT) and heat rejection for the direct system, as demonstrated in Fig. 20. In an indirect cooling system, for a fixed water mass flow, the cycle overcooled at lower PCIT and undercooled at PCIT higher than the design point. The water mass flow rate optimized to maintain a constant CIT at lower PCIT values. As expected, the heat rejection in the tower almost linearly increased with PCIT for both cooling systems. At higher PCIT values, the direct system achieved higher cycle efficiency. Recently, Sun et al. [117] performed experimentation with NDDCT to investigate the performance of spray assisted dry cooling technique to compensate for the performance degradation in hot climate conditions by precooling the inlet air. Indirect cooling circuit with water as secondary cooling media was considered. The dry-cooled SCO_2 power cycle simulation performed with experimental dataset. Duniam and Veeraragavan [118] also assessed the off-design performance of dry-cooled SCO_2 recompression cycle equipped with molten salt solar tower. Lock et al. [119] described a broad modelling approach of direct cooling of SCO_2 with air-cooled heat exchanger and the performance of forced draft and natural draft towers are compared at the off-design condition. The required air-cooled

Table 7
Thermodynamic states in RC and PC cycles.

| Process | RC Cycle | PC Cycle |
|----------------------|---|--|
| Compression | state 1 to state 2 (MC); state 8 to state 3(RC) | state 1 to state 2 (MC); state 9 to state 10 (PC); state 10 to state 3(RC) |
| Expansion | state 5 to state 6 (Turbine) | state 5 to state 6 (Turbine) |
| Heat addition | state 4 to state 5 (Primary heat exchanger) | state 4 to state 5 (Primary heat exchanger) |
| Heat rejection | state 8 to state 1 (NDDCT) | state 8 to state 9 (NDDCT-1); state 10 to state 1 (NDDCT-2) |
| Heat recovery at LTR | (state 3 to state 8) and (state 2 to state 3) | (state 3 to state 8) and (state 2 to state 3) |
| Heat recovery at LTR | (state 6 to state 7) and (state 3 to state 4) | (state 6 to state 7) and (state 3 to state 4) |

Table 8

Economic evaluation of finned tube heat exchanger and NDDCT [114,122,124].

| Finned tube Heat Exchanger | |
|--|--|
| Parameter | Equation |
| Fin cost per unit length, C_f | $C_f = \frac{\pi(d_f^2 - d_r^2)}{4} t_f \left(\frac{1}{P_f + t_f} + 1 \right) \rho_{al} C_{ual} + C_{af}$ ρ_{al} is the density of aluminum fin, C_{ual} (6 \$/kg) is the unit cost of aluminum and C_{af} is the fabrication cost (0.4 \$/kg). |
| Tube cost per unit length, C_t | $C_t = \frac{\pi[d_r^2 - (d_r - 2e_t)^2]}{4} \rho_{steel} C_{ut} + C_{at}$ ρ_{steel} is the density of steel, C_{ut} (1.6 \$/kg) is the unit cost and C_{at} (4 \$/kg) is the fabrication cost. |
| Total finned tube cost, C_{ft} | $C_{ft} = n_b n_r n_r H_{hx} (C_f + C_t)$ H_{hx} (0.2) is the length of heat exchanger |
| Heat exchanger header cost, C_{header} | $C_{header} = C_{ft} f_{header}$ f_{header} (0.8) is the weighting factor. |
| Heat exchanger labor cost, C_{labour} | $C_{labour} = (C_{ft} + C_{header}) f_{labour}$ f_{labour} (0.7) is the weighting factor. |
| The total cost of the heat exchanger, C_{he} | $C_{he} = (C_{ft} + C_{header} + C_{labour}) f_{he}$ f_{he} (1.2) is the weighting factor. |
| NDDCT | |
| Parameter | Equation |
| Tower shell cost, C_{shell} | $C_{shell} = \frac{2.4(D_3 + D_5)}{H_5} (1392.2H_5^2 - 31937H_5 + 10^6)$ |
| Foundation cost, $C_{foundation}$ | $C_{foundation} = f_{foundation} D_3$ $f_{foundation}$ is the foundation unit cost (23,372 \$/m). |
| Tower support cost, $C_{support}$ | $C_{support} = C_{foundation} f_{support}$ $f_{support}$ (0.6) is the weighting factor. |
| Tower labor cost, C_{labour} | $C_{labour} = (C_{shell} + C_{support} + C_{foundation}) f_{labour}$ f_{labour} (1.1) is the weighting factor of labor cost. |
| Total NDDCT cost, C_{tower} | $C_{tower} = (C_{shell} + C_{support} + C_{foundation} + C_{labour}) f_{tower}$ f_{tower} (1.2) is the weighting factor of tower cost. |
| Maintenance and Annual Cost | |
| Parameter | Equation |
| Maintenance cost, C_{MC} | $C_{MC} = 0.01C_{he} + 0.005C_{tower}$ |
| Fixed charged rate, K | $K = \frac{i(1+i)^n}{(1+i)^n - 1}$ i is interest rate (9%) and n is the payment years (30 years). |
| Annual cost, C_{annual} | $C_{annual} = K(C_{he} + C_{tower}) + C_{MC}$ |
| Specific investment cost, SIC | $SIC = \frac{(C_{he} + C_{tower})}{Q_{NDDCT}}$ in \$/kW |

heat exchanger area for recompression cycle was proposed while incorporating the influence of buoyancy.

5. Case study: cooling system design for recompression and partial cooling cycle

A case study is performed to design the NDDCT for the recompression and partial cooling SCO_2 power cycles. Based on the literature [5,14,69,120], these two layouts are identified for potential application in CSP plants. The power cycle simulation is accomplished with IPSEpro [121] and the methodology to design the NDDCT is adapted from Kroger [51]. The cooling mechanism in a supercritical cycle occurs in the proximity of the critical condition where the discrepancy of transport properties is prevalent. The earlier research already demonstrated the heat transfer mechanism of SCO_2 in the heat exchanger [24,78]. However, the thermodynamic analysis of NDDCT was conducted in isolation decoupled from the power block. Coupling the two in the same simulation reveals interesting dynamics. The heat input is assumed to be from the thermal store and can be varied to maintain a turbine inlet temperature of 650 °C. This assumption decouples the analysis from solar field design. Fig. 21 shows the plant layouts integrated with NDDCT. The partial cooling cycle employs an additional compressor and cooling tower. In the recompression cycle, the low-pressure turbine exhaust stream at the

Table 9

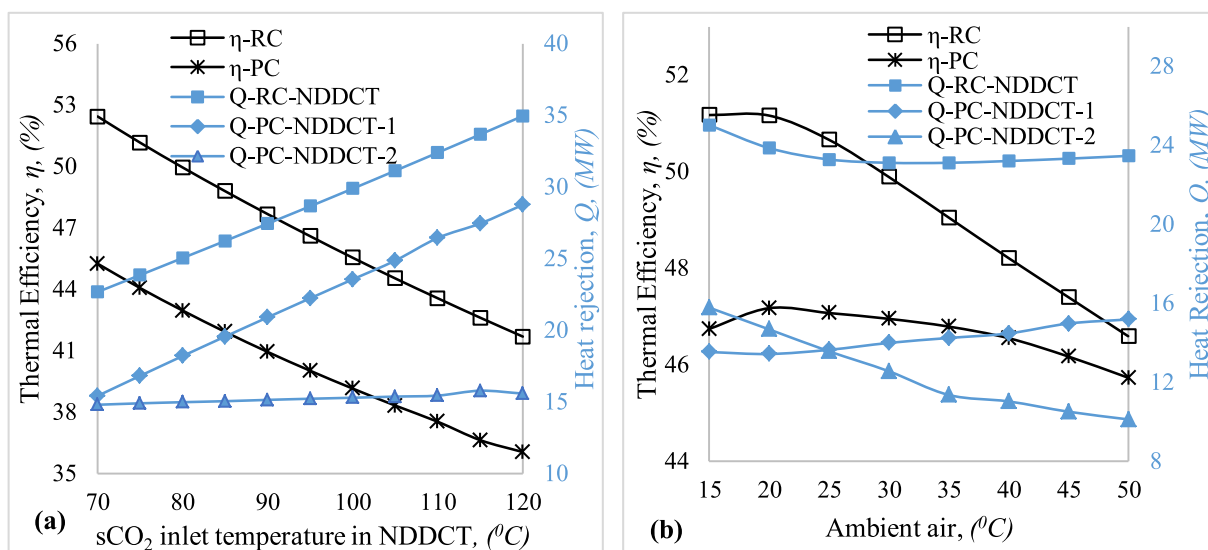
NDDCT size required for 25 MW recompression and partial cooling cycle.

| Parameter | Recompression Cycle | Partial Cooling Cycle | |
|--|-----------------------|-----------------------|-----------------------|
| | | NDDCT-1 | NDDCT-2 |
| Heat Rejected, Q | 23.8 MW | 14.68 MW | 13.43 MW |
| Outlet tower height, H_5 | 52.45 m | 38.7 m | 35.4 m |
| Unit height heat dissipation | 0.45 MW/m | 0.41 MW/m | 0.35 MW/m |
| Heat Exchanger height, H_4 | 6 m | 4.3 m | 4.1 m |
| Inlet tower height, H_3 | 5.76 m | 4.07 m | 3.72 m |
| Outlet diameter, d_5 | 26.22 m | 19.4 m | 17.7 m |
| Inlet diameter, d_3 | 37.46 m | 27.66 m | 25.25 m |
| Quantity of heat exchanger bundles, n_b | 22 | 12 | 10 |
| Quantity of NDDCT supports: n_{ts} | 27 | 20 | 18 |
| Support span: l_{ts} | 6.65 m | 4.92 m | 4.5 m |
| Frontal area of bundles, A_{fr} | 717 m ² | 358 m ² | 330 m ² |
| Air side area, A_a | 527127 m ² | 287524 m ² | 239603 m ² |
| Tube side area, A_t | 3924 m ² | 1961 m ² | 1808 m ² |
| Overall UA | 2159 kW/K | 1032 kW/K | 978 kW/K |
| Average Nusselt Number, Nu | 2082 | 1865 | 1711 |
| sCO ₂ inlet velocity, v_s | 0.95 m/s | 1.36 m/s | 1.45 m/s |
| sCO ₂ mean outlet temperature, T_{cf} | 33.2 °C | 40.1 °C | 39.8 °C |
| Economic Comparison (AUD \$) | | | |
| Total cost of the heat exchanger, C_{he} | 1,315,353 | 1,195,775 | 1,076,197 |
| Total NDDCT cost, C_{tower} | 10,635,022 | 10,246,278 | 11,075,19 |
| Maintenance cost, C_{MC} | 18471 | 17080 | 16297 |
| Specific investment cost, SIC | 502 \$/kW | 779 \$/kW | 904 \$/kW |

outlet of LTR is split. One path follows the NDDCT and the remaining is processed by the RC to the system higher pressure. However, in the partial cooling cycle, the NDDCT-1 cools the total mass of sCO₂ and after the PC the flow then splits. The NDDCT-2 cools a portion of the total mass determined by the split ratio. Both cycles work under cycle highest pressure of 20 MPa and pressure ratio of 2.5. For the partial cooling cycle, the intermediate pressure is optimized based on higher cycle efficiency and power generation and taken as 11 MPa. The NDDCT is designed to acquire the desired main compressor inlet temperature of 33 °C for the recompression cycle whereas for partial cooling cycles, both the cooling towers are designed to cool sCO₂ up to 40 °C. Table 7 represents the various thermodynamic states in the proposed power blocks.

The selection of the design point of NDDCT is evaluated based on the optimum operating condition of the power cycle. The power cycle modelling equations, simulation assumption, boundary conditions, and optimization of design parameters (pressure ratio and tower exit temperature) are outlined in our previously works [33,82]. In the simulation, the turbine and compressors are modelled by defining the adiabatic efficiency of 0.9 and 0.89 respectively. The pinch point constraint in the recuperators is taken as 5 °C. All the processes are performed under steady-state and the radiative heat loss is considered insignificant. The cooling towers are designed for a climate condition of 20 °C, 101.3 kPa, air velocity of 1 m/s, and relative humidity of 60%. Table 8, exhibits the cost correlations of dry cooling tower taken from the studies of Duniam [122], Zou et al. [114], and Conradie [123]. The cost model comprises the capital cost, maintenance cost, and annual cost with a 9% interest rate over 30 years repayment period. Table 9, reveals the cooling system specifications for both cycles applicable for solar thermal plant. The recompression cycle requires a tower with 52.4 m height while the partial cooling requires dual short towers of 38.7 m and 35.4 m height to accomplish the design point main compressor inlet temperature.

The cooling efficiency of tower is highly influenced by the cycle fluid inlet temperature and ambient condition. Fig. 22(a) demonstrates the power cycle performance with the variation of sCO₂ inlet temperature inside the cooling tower. Increasing the inlet temperature lowers the cycle efficiency for both cycles due to the requirement of higher thermal energy input to attain the same turbine inlet temperature. The RC cycle demonstrates superior efficiency compared to the PC cycle. The required solar energy input to the primary heat exchanger for the RC cycle augments from 47.6 MW to 59.9 MW while for the PC cycle 55.2 MW–69.3 MW. Rising the inlet temperature also enhances the heat rejection by the tower due to the higher initial temperature difference of sCO₂ and air. The heat dissipated by the recompression cycle intensifies from 22.6 MW to 34.9 MW. The heat rejection of NDDCT-1 of partial cooling cycle increases from 15.4 MW to 28.7 MW and for NDDCT-2, the value merely rises from 14.8 MW to 15.5 MW. However, the total heat rejected for both towers increases with the increase of sCO₂ temperature. Fig. 22(b) shows the cycle performance of both cycles with the variation of air temperature from 15 °C to 50 °C. The recompression cycle shows higher values in thermal efficiency compared to the partial cooling cycle due to the acquisition of the lower main compressor inlet temperature. The cycle efficiency for the RC cycle decreases from 52.1% to 46.5% and for the partial cooling cycle 46.7%–45.7%. The heat rejection for the recompression cycle decreases from 25 MW to 23.4 MW. For the PC cycle, the NDDCT-1 rejects heat of 13.5 MW–15.1 MW and for NDDCT-2,

**Fig. 22.** Thermal performance comparison of both cycles under the influence of (a) cycle fluid inlet temperature inside NDDCT and (b) air temperature.

the heat dissipation reduces from 15.7 MW to 10.1 MW. The total heat rejected by the PC cycle declines with air temperature. For PC cycle operating with two NDDCTs requires a complex operational strategy. From economic perspective, the RC cycle offers superiority in terms of lower specific investment cost. Based on the case study, the recompression cycle is recommended for forthcoming commercialization of dry-cooled CSP plants on large scale due to its less complication in cycle layout and reduced capital investment in designing the central receiver and heliostat field with a larger area.

6. Design recommendation for future dry-cooled CSP plant

The general guideline for future dry-cooled CSP plants operating with sCO₂ power block is as follows.

- The CSP plant power generation is strongly dominant by the variant climate conditions (solar irradiance and air temperature). Based on the CSP location, climate dataset must be taken into consideration while designing the NDDCT.
- Various sCO₂ power cycle layouts are reported in the literature to obtain the highest possible cycle efficiency; however, the recompression cycle is mostly recommended as a next-generation power block due to several potential benefits and ease of operation.
- The design parameter optimization for the solar field (mass flow, TES temperatures, and split ratio) and power cycle (pressure ratio, split ratio, and tower exit temperature) should be conducted before coupling the power block with NDDCT.
- The proper selection of climate temperature is crucial to maximizing the power generation at different seasonal conditions.
- The NDDCT geometry optimization should reflect the comprehensive economic assessment. Designing the air-cooled heat exchangers inside the tower requires additional precaution since the working fluid is sCO₂. The property variation must be taken into consideration by sectioning the heat exchangers into small segments.
- During extreme summer conditions, the performance degradation with NDDCT can be compensated by a supplementary cooling component (fan draft system, radiative cooler, wet cooling system, and hybrid cooling system). On the other hand, during extreme winter conditions, a supplementary flow splitter could be installed prior to NDDCT to reduce the heat rejection and prevent cycle overcooling. Maintaining the supercritical state of the working fluid is necessary to avoid any instabilities with compressors.

7. Conclusion

The present review work highlights the potential advantages of dry cooling component equipped with sCO₂ power cycles in the solar

application. In steam power generation, dry cooling is generally not favored due to the steam condensation issue, higher irreversibility and thermal losses, and requirement of higher air mass flow rate which considerably augments the power consumption. However, recent research studies have identified the potential benefits of dry cooling working with sCO₂. The smoother sCO₂ cooling profile corresponds to lower exergy losses and the extra degree of freedom in the sCO₂ cycles in terms of the lower cycle pressure helps maintaining the power cycle efficiency at high ambient temperatures. In the likely future CSP plant locations, fresh water supply is a great challenge. Therefore, a cycle that is more suitable for dry cooling is better for CSP applications. Other factors also favor dry cooling over the wet cooling system, with concerns on corrosion, dissolved solids, scale deposition, and unwanted and unexpected accumulation of sediments.

A plethora of research articles has signified the acquirement of the higher cycle efficiency with various sCO₂ power cycle layouts using dry cooling. Few studies from the literature have been identified which highlight the performance enhancement of dry-cooled sCO₂ power cycles at the off-design condition. The employment of an extremum seeking controller, the hybrid cooling approach, and the radiative cooling as an additional cooling component can recompense the performance degradation during high climate temperature period.

This paper addressed detailed thermodynamic modelling of a dry-cooled sCO₂ power block with a detailed cost assessment of a dry cooling system. Preliminary analysis to design the cooling system is performed for the recompression cycle and the partial cooling cycle with a detailed modelling approach. Heat exchangers are discretized into small segments to predict the property variation of sCO₂ with the decrease of the bulk temperature. The recompression cycle shows higher values in cycle efficiency with the variation of sCO₂ inlet temperature in the tower and ambient temperature. The analysis carried out in the present work shows a pathway in designing the dry cooling system for supercritical CO₂ power cycles based on the optimal operational condition.

Declaration of competing interest

Authors have no conflict of interests.

Acknowledgment

Thanks to the University of Queensland (UQ) for granting Research Training Program scholarship. This research is a part of the Australia Solar Thermal Research Initiative (ASTRI), a project provided by the Australia Government, through the Australia Renewable Energy Agency (ARENA).

Nomenclature

| | |
|------------------|---|
| A | Area, m ² |
| C _p | Specific heat, J/kgK |
| C _{Dts} | Drag coefficient |
| D | Diameter, m |
| f | Friction factor |
| F _T | Correction factor |
| F _{Dts} | Drag force, N |
| G | Mass velocity, kg/m ² s |
| h | Heat transfer coefficient, W/m ² K |
| H | Height, m |
| k | Thermal conductivity, W/mK |
| K | Loss coefficient |
| L _t | Length of tube, m |
| M | Total mass flow rate, kg/s |

| | |
|-----------------|-------------------------------------|
| n _{ts} | Number of supports |
| n _r | Number of rows |
| n _{tr} | Effective no of tubes per row |
| P _f | Fin pitch, m |
| P _t | Transversal pitch, m |
| P _l | Longitudinal pitch, m |
| P _d | Diagonal pitch, m |
| P _{cr} | Critical Pressure, N/m ² |
| Q | Heat transfer rate, W |
| q | Heat flux, W/m ² |
| T | Temperature, °C or K |
| t _f | Fin thickness, m |
| t _{ft} | Tip thickness, m |
| t _{fr} | Root thickness, m |

Greek Symbols

| | |
|------------|----------------------------|
| ϵ | Surface roughness, m |
| η | Efficiency |
| μ | Dynamic viscosity, kg/ms |
| ρ | Density, kg/m ³ |
| σ | Area ratio |

Dimensionless Number

| | |
|-----------------|-------------------------------|
| F _{rD} | Froude number |
| P _r | Prandtl Number |
| R _e | Reynolds Number |
| R _y | Characteristic Reynold number |

Subscript

| | |
|-----|---------------------------------|
| a | air side |
| ct | cooling tower |
| ctc | cooling tower contraction |
| cte | cooling tower expansion |
| cv | control volume |
| f | fin |
| frT | frontal |
| he | heat exchanger |
| i | inner; inlet |
| o | outer; outlet |
| lm | log mean temperature difference |
| pc | Pseudocritical |
| r | root |
| s | Supercritical |
| si | sCO ₂ inlet |
| so | sCO ₂ outlet |
| to | tower outlet |
| ts | tower support |

References

- [1] A. E. S. p. team. Australian energy update. In: Energy statistics and analysis section. Australia2018: Department of the Environment and Energy; 2018.
- [2] Dostal V, Driscoll MJ, Hejzlar P, Todreas NE. A supercritical CO₂ gas turbine power cycle for next-generation nuclear reactors. Proc. of ICONE 2002;10. 2002.
- [3] Dostal V, Hejzlar P, Driscoll MJ. The supercritical carbon dioxide power cycle: comparison to other advanced power cycles. Nucl Technol 2006;154(3):283–301.
- [4] Persichilli M, Kacludis A, Zdankiewicz E, Held T. Supercritical CO₂ power cycle developments and commercialization: why sCO₂ can displace steam ste. Power-Gen India & Central Asia 2012;2012:19–21.
- [5] Besarati SM, Goswami DY. Analysis of advanced supercritical carbon dioxide power cycles with a bottoming cycle for concentrating solar power applications. J Sol Energy Eng 2014;136(1):010904.
- [6] Ehsan MM, Guan Z, Klimentko A. A comprehensive review on heat transfer and pressure drop characteristics and correlations with supercritical CO₂ under heating and cooling applications. Renew Sustain Energy Rev 2018;92:658–75.
- [7] Dang C, Hihara E. In-tube cooling heat transfer of supercritical carbon dioxide. Part 1. Experimental measurement. Int J Refrig 2004;27(7):736–47.
- [8] Huai X, Koyama S, Zhao T. An experimental study of flow and heat transfer of supercritical carbon dioxide in multi-port mini channels under cooling conditions. Chem Eng Sci 2005;60(12):3337–45.
- [9] Li H, et al. Development of a new forced convection heat transfer correlation for CO₂ in both heating and cooling modes at supercritical pressures. Int J Therm Sci 2011;50(12):2430–42.
- [10] Garg P, Srinivasan K, Dutta P, Kumar P. Comparison of CO₂ and steam in transcritical Rankine cycles for concentrated solar power. Energy Procedia 2014; 49:1138–46.
- [11] Dunham MT, Iverson BD. High-efficiency thermodynamic power cycles for concentrated solar power systems. Renew Sustain Energy Rev 2014;30:758–70.
- [12] Wang K, Li M-J, Guo J-Q, Li P, Liu Z-B. A systematic comparison of different S-CO₂ Brayton cycle layouts based on multi-objective optimization for applications in solar power tower plants. Appl Energy 2018;212:109–21.
- [13] Shi L, et al. Experimental investigation of a CO₂-based transcritical Rankine cycle (CTRC) for exhaust Gas Recovery. Energy; 2018.
- [14] Neises T, Turchi C. A comparison of supercritical carbon dioxide power cycle configurations with an emphasis on CSP applications. Energy Procedia 2014;49: 1187–96.

- [15] Ma Z, Turchi CS. Advanced Supercritical Carbon Dioxide Power cycle configurations for Use in concentrating Solar Power Systems: Preprint. Golden, CO: National Renewable Energy Laboratory (NREL); 2011.
- [16] Cheng L, Ribatski G, Thome JR. Analysis of supercritical CO₂ cooling in macro- and micro-channels. *Int J Refrig* 2008;31(8):1301–16.
- [17] Dostál V, Driscoll M, Hejzlar P. A Supercritical Carbon Dioxide cycle for Next Generation Nuclear Reactors. Massachusetts Institute of Technology; 2004.
- [18] Conboy T, Carlson M, Rochau G. Dry-cooled supercritical CO₂ power for advanced nuclear reactors. *J Eng Gas Turbines Power* 2015;137(1):012901.
- [19] Zeygami M, Khalili F. Performance improvement of dry cooled advanced concentrating solar power plants using daytime radiative cooling. *Energy Convers Manag* 2015;106:10–20.
- [20] Ho CK, Carlson M, Garg P, Kumar P. Technoeconomic analysis of alternative solarized s-CO₂ Brayton cycle configurations. *J Sol Energy Eng* 2016;138(5):051008.
- [21] Milani D, Luu MT, McNaughton R, Abbas A. Optimizing an advanced hybrid of solar-assisted supercritical CO₂ Brayton cycle: a vital transition for low-carbon power generation industry. *Energy Convers Manag* 2017;148:1317–31.
- [22] Luu MT, Milani D, McNaughton R, Abbas A. Dynamic modelling and start-up operation of a solar-assisted recompression supercritical CO₂ Brayton power cycle. *Appl Energy* 2017;199:247–63.
- [23] Son S, Lee JI. Application of adjoint sensitivity analysis method to supercritical CO₂ power cycle optimization. *Energy* 2018;147:1153–64.
- [24] Ehsan MM, Guan Z, Klimenko A, Wang X. Design and comparison of direct and indirect cooling system for 25 MW solar power plant operated with supercritical CO₂ cycle. *Energy Convers Manag* 2018;168:611–28.
- [25] Duniam S, Jahn I, Hooman K, Lu Y, Veeraraghavan A. Comparison of direct and indirect natural draft dry cooling tower cooling of the sCO₂ Brayton cycle for concentrated solar power plants. *Appl Therm Eng* 2018;130:1070–80.
- [26] Dai Y, Wang X, Li X, Guan Z, Dai Y. Preliminary analysis of direct and indirect heat rejection systems for a small sCO₂ Brayton cycle using an existing natural draft dry cooling tower. *J Energy Eng* 2018;144(2):04018005.
- [27] Padilla RV, Too YCS, Beath A, McNaughton R, Stein W. Effect of pressure drop and reheating on thermal and exergetic performance of supercritical carbon dioxide Brayton cycles integrated with a solar central receiver. *J Sol Energy Eng* 2015;137(5):051012.
- [28] Padilla RV, Benito R, Stein W. An exergy analysis of recompression supercritical CO₂ cycles with and without reheating. *Energy Procedia* 2015;69:1181–91.
- [29] Padilla RV, Too YCS, Benito R, Stein W. Exergetic analysis of supercritical CO₂ Brayton cycles integrated with solar central receivers. *Appl Energy* 2015;148:348–65.
- [30] Osorio JD, Hovsapian R, Ordóñez JC. Dynamic analysis of concentrated solar supercritical CO₂-based power generation closed-loop cycle. *Appl Therm Eng* 2016;93:920–34.
- [31] Ma Y, Zhang X, Liu M, Yan J, Liu J. Proposal and assessment of a novel supercritical CO₂ Brayton cycle integrated with LiBr absorption chiller for concentrated solar power applications. *Energy* 2018;148:839–54.
- [32] Linares JI, Montes MJ, Cantizano A, Sánchez C. A novel supercritical CO₂ recompression Brayton power cycle for power tower concentrating solar plants. *Appl Energy* 2020;263:114644.
- [33] Ehsan MM, Duniam S, Li J, Guan Z, Gurgenci H, Klimenko A. A comprehensive thermal assessment of dry cooled supercritical CO₂ power cycles. *Appl Therm Eng* 2020;166:114645.
- [34] Ehsan MM, Guan Z, Gurgenci H, Klimenko A. Novel design measures for optimizing the yearlong performance of a concentrating solar thermal power plant using thermal storage and a drycooled supercritical CO₂ power block. *Energy Convers Manag* 2020;216:112980.
- [35] Wang X, Li X, Li Q, Liu L, Liu C. Performance of a solar thermal power plant with direct air-cooled supercritical carbon dioxide Brayton cycle under off-design conditions. *Appl Energy* 2020;261:114359.
- [36] Ahn Y, et al. Review of supercritical CO₂ power cycle technology and current status of research and development. *Nuclear Engineering and Technology* 2015;47(6):647–61.
- [37] Ahn Y, Lee J, Kim SG, Lee JI, Cha JE, Lee S-W. Design consideration of supercritical CO₂ power cycle integral experiment loop. *Energy* 2015;86:115–27.
- [38] Kumar P, Srinivasan K. Carbon dioxide based power generation in renewable energy systems. *Appl Therm Eng* 2016;109:831–40.
- [39] Sarkar J. Review and future trends of supercritical CO₂ Rankine cycle for low-grade heat conversion. *Renew Sustain Energy Rev* 2015;48:434–51.
- [40] Crespi F, Gavagnin G, Sánchez D, Martínez GS. Supercritical carbon dioxide cycles for power generation: a review. *Appl Energy* 2017;195:152–83.
- [41] Li M-J, Zhu H-H, Guo J-Q, Wang K, Tao W-Q. The development technology and applications of supercritical CO₂ power cycle in nuclear energy, solar energy and other energy industries. *Appl Therm Eng* 2017;126:255–75.
- [42] Cheng L, Ribatski G, Thome JR. Analysis of supercritical CO₂ cooling in macro- and micro-channels. *Int J Refrig* 2008;31(8):1301–16.
- [43] Lin W, Du Z, Gu A. Analysis on heat transfer correlations of supercritical CO₂ cooled in horizontal circular tubes. *Heat Mass Tran* 2012;48(4):705–11.
- [44] Surendran P, Gupta S, Preda T, Pioro I. Comparison OF existing SUPERCRITICAL carbon dioxide heat TRANSER correlations for horizontal and vertical bare tubes. In: 2012 20th international conference on nuclear engineering and the ASME 2012 power conference. American Society of Mechanical Engineers; 2012. p. 335–42.
- [45] Pioro IL, Khatabil HF, Duffey RB. Heat transfer to supercritical fluids flowing in channels—empirical correlations (survey). *Nucl Eng Des* 2004;230(1):69–91.
- [46] Gupta S, McGillivray D, Surendran P, Trevani L, Pioro I. Developing heat-transfer correlations for supercritical CO₂ flowing in vertical bare tubes. In: Proceedings of ICONE20-power2012. Anaheim, CA; July; 2012.
- [47] Gupta S, Mokry S, Pioro I. Developing a heat-transfer correlation for supercritical water flowing in vertical tubes and its application in SCWRs. 2011.
- [48] Fang X, Xu Y. Modified heat transfer equation for in-tube supercritical CO₂ cooling. *Appl Therm Eng* 2011;31(14–15):3036–42.
- [49] Cabeza LF, de Gracia A, Fernández AI, Farid MM. Supercritical CO₂ as heat transfer fluid: a review. *Appl Therm Eng* 2017;125:799–810.
- [50] Vignarooban K, Xu X, Arvay A, Hsu K, Kannan A. Heat transfer fluids for concentrating solar power systems—a review. *Appl Energy* 2015;146:383–96.
- [51] Kröger DG. Air-cooled heat exchangers and cooling towers. PennWell Books; 2004.
- [52] Terblanche J, Kröger D. Experimental evaluation of the aerodynamic inlet losses in cooling towers. *S. Afr. Inst. Mech. Eng. R&D J* 1994;10(2):41–4.
- [53] Du Preez A, Kröger D. The influence of buoyant plume on the performance of a natural draft cooling tower. In: 9th IAHR cooling tower and spraying pond symposium; 1994. Brussels.
- [54] Geldenhuys J, Kröger D. Aerodynamic inlet losses in natural draft cooling towers. In: Proceedings of the 5th IAHR cooling tower workshop; 1986.
- [55] Du Preez A, Kröger D. Experimental evaluation of aerodynamic inlet losses in natural draft dry cooling towers. 1989.
- [56] Vauzanges M, Ribier G. Variation of the head losses in the air inlets of natural draft cooling towers with the shape of the lintel and shell supports. In: Proc. 5th IAHR cooling tower workshop; 1986.
- [57] Briggs DE, Young EH. Convection heat transfer and pressure drop of air flowing across triangular pitch banks of finned tubes. *Chem Eng Prog Symp Ser* 1963;59(41):1–10.
- [58] Vampola J. Heat transfer and pressure drop in flow of gases across finned tube banks. *Strojirenstvi* 1966;7:501–7.
- [59] Mirkovic Z. Heat transfer and flow resistance correlation for helically finned and staggered tube banks in crossflow. In: Heat exchangers: design and theory source book; 1974. p. 559–84.
- [60] Ganguli A, Tung S, Taborek J. Parametric study of air-cooled heat exchanger finned tube geometry. *AICHE Symp Ser* 1985;81:122–8.
- [61] Rabas T, Eckels P, Sabatino R. The effect of fin density on the heat transfer and pressure drop performance of low-finned tube banks. *Chem Eng Commun* 1981;10(1–3):127–47.
- [62] Wang C-C, Chang Y-J, Hsieh Y-C, Lin Y-T. Sensible heat and friction characteristics of plate fin-and-tube heat exchangers having plane fins. *Int J Refrig* 1996;19(4):223–30.
- [63] Gianolio E, Cuti F. Heat transfer coefficients and pressure drops for air coolers with different numbers of rows under induced and forced draft. *Heat Tran Eng* 1981;3(1):38–48.
- [64] Wang C-C, Chi K-Y, Chang C-J. Heat transfer and friction characteristics of plain fin-and-tube heat exchangers, part II: Correlation. *Int J Heat Mass Tran* 2000;43(15):2693–700.
- [65] Robinson KK, Briggs DE. Pressure drop of air flowing across triangular pitch banks of finned tubes. *Chem Eng Prog Symp Ser* 1966;62(64):177–84.
- [66] Nir A. Heat transfer and friction factor correlations for crossflow over staggered finned tube banks. *Heat Tran Eng* 1991;12(1):43–58.
- [67] Jacob M. Heat transfer and flow resistance in cross flow of gases over tube banks. *Trans. ASME* 1938;60(38):384–6.
- [68] Kim N, Youn B, Webb R. Air-side heat transfer and friction correlations for plain fin-and-tube heat exchangers with staggered tube arrangements. *J Heat Tran* 1999;121(3):662–7.
- [69] Turchi CS, Ma Z, Neises TW, Wagner MJ. Thermodynamic study of advanced supercritical carbon dioxide power cycles for concentrating solar power systems. *J Sol Energy Eng* 2013;135(4):041007.
- [70] Dyreby J, Klein S, Nellis G, Reindl D. Design considerations for supercritical carbon dioxide Brayton cycles with recompression. *J Eng Gas Turbines Power* 2014;136(10):101701.
- [71] Moiseyev A, Sienicki JJ. Investigation of a dry air cooling option for an S-CO₂ cycle. In: Supercritical CO₂ power symposium; 2014. Pittsburgh (PA), Sep 9e10.
- [72] Hu L, et al. Investigation on the performance of the supercritical Brayton cycle with CO₂-based binary mixture as working fluid for an energy transportation system of a nuclear reactor. *Energy* 2015;89:874–86.
- [73] Ma Y, Liu M, Yan J, Liu J. Thermodynamic study of main compression intercooling effects on supercritical CO₂ recompression Brayton cycle. *Energy* 2017;140:746–56.
- [74] Li L, Ge Y, Luo X, Tassou SA. Experimental investigation on power generation with low grade waste heat and CO₂ transcritical power cycle. *Energy Procedia* 2017;123:297–304.
- [75] Pidaparti SR, Moiseyev A, Sienicki JJ, Ranjan D. Counter flow induced draft cooling tower option for supercritical carbon dioxide Brayton cycle. *Nucl Eng Des* 2015;295:549–58.
- [76] Singh R, Kearney MP, Manzie C. Extremum-seeking control of a supercritical carbon-dioxide closed Brayton cycle in a direct-heated solar thermal power plant. *Energy* 2013;60:380–7.
- [77] Singh R, Miller SA, Rowlands AS, Jacobs PA. Dynamic characteristics of a direct-heated supercritical carbon-dioxide Brayton cycle in a solar thermal power plant. *Energy* 2013;50:194–204.
- [78] Ehsan MM, Wang X, Guan Z, Klimenko A. Design and performance study of dry cooling system for 25 MW solar power plant operated with supercritical CO₂ cycle. *Int J Therm Sci* 2018;132:398–410.

- [79] Ehsan MM, Duniam S, Li J, Guan Z, Gurgenci H, Klimenko A. Effect of cooling system design on the performance of the recompression CO₂ cycle for concentrated solar power application. *Energy* 2019;180:480–94.
- [80] Moisseytsev A, Sienicki JJ. Investigation of a dry air cooling option for an S-CO₂ cycle. In: Supercritical CO₂ power symposium; 2014. Pittsburgh (PA).
- [81] Cheng W-L, Huang W-X, Nian Y-L. Global parameter optimization and criterion formula of supercritical carbon dioxide Brayton cycle with recompression. *Energy Convers Manag* 2017;150:669–77.
- [82] Ehsan MM, Duniam S, Li J, Guan Z, Gurgenci H, Klimenko A. Effect of cooling system design on the performance of the recompression CO₂ cycle for concentrated solar power application. *Energy* 2019;180:480–94.
- [83] Ehsan MM, Duniam S, Guan Z, Gurgenci H, Klimenko A. Seasonal variation on the performance of the dry cooled supercritical CO₂ recompression cycle. *Energy Convers Manag* 2019;197:111865.
- [84] Matraji I, Ahmed FS, Laghrouche S, Wack M. Extremum seeking control for net power output maximization of a PEM fuel cell using second order sliding mode. In: Variable structure systems (VSS), 2012 12th international workshop on. IEEE; 2012. p. 331–6.
- [85] Bizon N. Energy harvesting from the PV hybrid power source. *Energy* 2013;52:297–307.
- [86] Li X, Li Y, Seem JE, Li P. Dynamic modeling and self-optimizing operation of chilled water systems using extremum seeking control. *Energy Build* 2013;58:172–82.
- [87] Pan T, Ji Z, Jiang Z. Maximum power point tracking of wind energy conversion systems based on sliding mode extremum seeking control. In: Energy 2030 conference. ENERGY 2008. IEEE; 2008. 2008, pp. 1–5; IEEE.
- [88] Luu MT, Milani D, McNaughton R, Abbas A. Advanced control strategies for dynamic operation of a solar-assisted recompression supercritical CO₂ Brayton power cycle. *Appl Therm Eng* 2018;136:682–700.
- [89] Narayanaswamy A, Chen G. Thermal emission control with one-dimensional metallo dielectric photonic crystals. *Phys Rev B* 2004;70(12):125101.
- [90] Rephaeli E, Fan S. Absorber and emitter for solar thermo-photovoltaic systems to achieve efficiency exceeding the Shockley-Queisser limit. *Optic Express* 2009;17(17):15145–59.
- [91] Rephaeli E, Raman A, Fan S. Ultrabroadband photonic structures to achieve high-performance daytime radiative cooling. *Nano Lett* 2013;13(4):1457–61.
- [92] Granqvist C, Hjortsberg A. Radiative cooling to low temperatures: general considerations and application to selectively emitting SiO films. *J Appl Phys* 1981;52(6):4205–20.
- [93] Catalanotti S, Cuomo V, Piro G, Ruggi D, Silvestrini V, Troise G. The radiative cooling of selective surfaces. *Sol Energy* 1975;17(2):83–9.
- [94] Al-Nimr M, Kodah Z, Nassar B. A theoretical and experimental investigation of a radiative cooling system. *Sol Energy* 1998;63(6):367–73.
- [95] Kimball B. Cooling performance and efficiency of night sky radiators. *Sol Energy* 1985;34(1):19–33.
- [96] Orel B, Gunde MK, Krainer A. Radiative cooling efficiency of white pigmented paints. *Sol Energy* 1993;50(6):477–82.
- [97] Nilsson TM, Niklasson GA. Radiative cooling during the day: simulations and experiments on pigmented polyethylene cover foils. *Sol Energy Mater Sol Cell* 1995;37(1):93–118.
- [98] Raman AP, Anoma MA, Zhu L, Rephaeli E, Fan S. Passive radiative cooling below ambient air temperature under direct sunlight. *Nature* 2014;515(7528):540.
- [99] Nilsson TM, Niklasson GA, Granqvist C-G. Solar-reflecting material for radiative cooling applications: ZnS pigmented polyethylene. Optical materials technology for energy efficiency and solar energy conversion XI: selective materials, concentrators and reflectors, transparent insulation and superwindows, vol. 1727. International Society for Optics and Photonics; 1992. p. 249–62.
- [100] Gentle AR, Smith GB. Radiative heat pumping from the earth using surface phonon resonant nanoparticles. *Nano Lett* 2010;10(2):373–9.
- [101] Zeyghami M, Goswami DY, Stefanakos E. A review of clear sky radiative cooling developments and applications in renewable power systems and passive building cooling. *Sol Energy Mater Sol Cell* 2018;178:115–28.
- [102] Wagner MJ, Kutscher C. The impact of hybrid wet/dry cooling on concentrating solar power plant performance. In: ASME 2010 4th international conference on energy sustainability. American Society of Mechanical Engineers; 2010. p. 675–82.
- [103] Barigozzi G, Perdichizzi A, Ravelli S. Wet and dry cooling systems optimization applied to a modern waste-to-energy cogeneration heat and power plant. *Appl Energy* 2011;88(4):1366–76.
- [104] Barigozzi G, Perdichizzi A, Ravelli S. Performance prediction and optimization of a waste-to-energy cogeneration plant with combined wet and dry cooling system. *Appl Energy* 2014;115:65–74.
- [105] Rezaei E, Shafiei S, Abdollahnezhad A. Reducing water consumption of an industrial plant cooling unit using hybrid cooling tower. *Energy Convers Manag* 2010;51(2):311–9.
- [106] Sadafi M, et al. An investigation on spray cooling using saline water with experimental verification. *Energy Convers Manag* 2016;108:336–47.
- [107] Sadafi M, Jahn I, Hooman K. Cooling performance of solid containing water for spray assisted dry cooling towers. *Energy Convers Manag* 2015;91:158–67.
- [108] Alkhedhair A, Gurgenci H, Jahn I, Guan Z, He S. Numerical simulation of water spray for pre-cooling of inlet air in natural draft dry cooling towers. *Appl Therm Eng* 2013;61(2):416–24.
- [109] Alkhedhair AMS. Modelling and experimental study of spray cooling systems for inlet air pre-cooling in natural draft dry cooling towers. 2015.
- [110] Alkhedhair A, Guan Z, Jahn I, Gurgenci H, He S. Water spray for pre-cooling of inlet air for natural draft dry cooling towers—experimental study. *Int J Therm Sci* 2015;90:70–8.
- [111] Goodarzi M, Keimanesh R. Heat rejection enhancement in natural draft cooling tower using radiator-type windbreakers. *Energy Convers Manag* 2013;71:120–5.
- [112] Zou Z, Guan Z, Gurgenci H, Lu Y. Solar enhanced natural draft dry cooling tower for geothermal power applications. *Sol Energy* 2012;86(9):2686–94.
- [113] Zou Z, He S. Modeling and characteristics analysis of hybrid cooling-tower-solar-chimney system. *Energy Convers Manag* 2015;95:59–68.
- [114] Zou Z, Guan Z, Gurgenci H. Optimization design of solar enhanced natural draft dry cooling tower. *Energy Convers Manag* 2013;76:945–55.
- [115] Ghorbani B, Ghashami M, Ashjaee M, Hosseinzadegan H. Electricity production with low grade heat in thermal power plants by design improvement of a hybrid dry cooling tower and a solar chimney concept. *Energy Convers Manag* 2015;94:1–11.
- [116] Ehsan MM, Guan Z, Gurgenci H, Klimenko AY. Irreversibility and exergy analysis OF a recompression supercritical CO₂ cycle coupled with dry cooling system. In: ASTFE digital library. Begel House Inc; 2019.
- [117] Sun Y, et al. Coupling supercritical carbon dioxide Brayton cycle with spray-assisted dry cooling technology for concentrated solar power. *Appl Energy* 2019;251:113328.
- [118] Duniam S, Veeraragavan A. Off-design performance of the supercritical carbon dioxide recompression Brayton cycle with NDDCT cooling for concentrating solar power. *Energy* 2019;187:115992.
- [119] Lock A, Hooman K, Guan Z. A detailed model of direct dry-cooling for the supercritical carbon dioxide Brayton power cycle. In: Applied thermal engineering; 2019. p. 114390.
- [120] Al-Sulaiman FA, Atif M. Performance comparison of different supercritical carbon dioxide Brayton cycles integrated with a solar power tower. *Energy* 2015;82:61–71.
- [121] IPSEpro S. Process Simulation environment (PSE). Austria: Simtech; 2003.
- [122] Duniam S. Design optimisation of an Australian EGS power plant using a natural draft dry cooling tower. 2016.
- [123] Conradie A, Kröger D. Performance evaluation of dry-cooling systems for power plant applications. *Appl Therm Eng* 1996;16(3):219–32.
- [124] Conradie AE. Performance optimization of engineering systems with particular reference to dry-cooled power plants. Stellenbosch: University of Stellenbosch; 1995.